LASER LIGHT SCATTERING AS A PLASMA DIAGNOSTIC TECHNIQUE

Alfred Anthony Pease

United States
Naval Postgraduate School

THESIS

LASER LIGHT SCATTERING AS A PLASMA
DIAGNOSTIC TECHNIQUE

by

Alfred Anthony Pease

June 1969

Laser Light Scattering As a Plasma Diagnostic Technique

by

Alfred Anthony Pease
Lieutenant (junior grade), United States Navy
B.S. United States Naval Academy, 1968

Submitted in partial fulfillment of the
requirements for the degree of

MASTER OF SCIENCE IN PHYSICS

from the

NAVAL POSTGRADUATE SCHOOL
June 1969

ABSTRACT

The effort here was concerned with initiating a long term experimental study to develop the method of laser light scattering as a plasma diagnostic technique. This was done with a ruby laser and a grating spectometer coupled with sensitive detectors, at the steady state plasma facility at the Naval Postgraduate School. Although attempts to detect the extremely low levels of scattered light failed, excellent progress was made in determining existing apparatus limitations and in recognizing which system parameter may be adjusted in order to detect the scattered light; this will enable the future experimenter to progress with a minimum of overlap.

TABLE OF CONTENTS

LIST OF DRAWINGS AND PHOTOGRAPHS

ACKNOWLEDGEMENT

I am deeply indebted to Professor Fred Schwirzke, whose untiring assistance and patience made this paper possible.

An especially warm and heartfelt thanks to Hal Herreman, without whom all activity in the Plasma Laboratory would have come to a standstill. If equipment failed or did not work properly, he knew the cause (always simply "malfunction") and could remedy the situation rapidly. There were two technicians who were absolutely indispensable in that laboratory; Hal was both of them. Next I extend my thanks to Pete Wisler, our machinist whose deft hand was responsible for a good many of the contraptions I justified as equipment in the name of science.

My warm thanks also to the lovely Deborah Singleton, who bravely attacked and admirably interpreted my illegible handscribble to spend long hours typing a first draft for me. A hearty thanks to that professional among professionals, Mr. Roy A. Puleo, whose devotion to perfection produced the fine typographical result you see here.

And since only mothers read this, the only sentimental aspect of an otherwise cold and impersonal report, I wish to thank my mother.

Finally, and so the true sentimentalist won't find the jump from this heartrending diversion to that mean report out there too much to bear without adequate preparation, I wish to thank the Navy...

I. INTRODUCTION

This thesis is intended as a detailed report of the beginning of a long-term experimental effort to develop Thomson scattering of laser beams as a plasma diagnostic technique. The technique employs the particle-like behavior of photons in scattering off plasma electrons. In general the background radiation from an energetic plasma dominates making it impossible to distinguish the scattered light. This problem may be somewhat alleviated by the use of an extremely intense, sharply tuned source in conjunction with narrow band detectors. The high power ruby laser is such a source and a grating spectrograph-photo multiplier tube arrangement is such a detector. Even with these improvements, a manifold of problems and complications yet exist, not the least of which is careful planning of the geometry of the experiments and associated alignment of apparatus. Previous experiments have shown that laser scattering from electron beams of energy approximately 2 kev and density approximately 5×10^{9} cm^{-3} yielded scattering intensities of only about 10^{-18} of the laser output. Though electron densities in the plasma under study are significantly higher, this gives some idea as to the problems presented in discerning the scattered light.

It will be shown that the spectral distribution of the scattered light is in part determined by a dimensionless coherence parameter proportional to the ratio of incident light wavelength to the Debye length;

$$\alpha \propto \frac{\lambda}{\lambda_o}$$

when α is small, that is, when the wavelength of incident light is small compared with the Debye length the cross section is the appropriate Thomson cross section and the shape of the scattered spectrum is a Gaussian; the width is the Doppler width associated with electron motion and as such is a measure of electron temperature.

When α is large ($\alpha >> 1$) the spectrum has a central line of the incident light frequency, ω_o, between two satellite peaks at frequencies $\omega_o + \omega_p$ where ω_p is the plasma frequency. In this case the Doppler broadening of the central peak is approximately proportional to the ion motion and gives information concerning ion temperatures.

The research begun in the plasma laboratory of the Naval Postgraduate School has been under the cognizance of Professor F. Schwirzke and is financed under Naval Air System Command Research Grant. The accomplishments made thus far and described herein will enable to the future experimenter to progress with a minimum of overlap. The major obstacle yet to be overcome, and indeed the main problem

in the development of this diagnostic method as a whole, is detecting the scattered light and distinguishing it from natural background radiation. Once this is done, the technique may be rapidly and effectively developed.

The diagnostic technique once developed, it may be employed to investigate turbulence in a laser produced plasma.

II. METHOD AND THEORY

A. ELECTROMAGNETIC THEORY OF LIGHT SCATTERING

Following directly from the equation of motion the amplitude of an electron oscillation caused by the electric field $\underline{E}'$ of the incident electromagnetic wave of frequency ω_o is;

$$\underline{S}(t) = \frac{e\,\underline{E}'(t)}{m\,\omega_o^2} = \frac{e\lambda^2 E'(t)}{4\pi^2 mc^2} \tag{1}$$

Multiplying the displacement by the electron charge e the induced dipole moment is obtained;

$$\underline{p} = -e\underline{s} = \frac{-e^2\lambda^2\underline{E}'}{4\pi^2 mc^2} = \epsilon\underline{E}' \tag{2}$$

For the laser light scattering to be dealt with here, is a plane monochromatic wave cut off exponentially at time $T = 1/\gamma$, the pulsetime constant.

That is,

$$\underline{E}'(r,t) = \underline{E}' \exp\{i[\underline{k}'\cdot\underline{r} + (\omega_o + i\gamma)t]\} \tag{3}$$

$$\underline{p}(r,t) = \epsilon\underline{E}'\exp\{i[\underline{k}'\cdot\underline{r} + (\omega_o + i\gamma)t]\} \tag{4}$$

It is this time dependent Dipole moment (4) which produces the scattered radiation.

The electric field $E_j''(r,t)$ scattered by the j^{th} electron at position r_j detected at $\mathcal{R}$, from the Hertz formula for dipole radiation, is

$$\underline{E}_j''(\mathcal{R},t) = f_j(\mathcal{R}_j,t)\exp[i(\underline{k}'\cdot\underline{r}_j + k'R_j) \tag{5}$$

$$\underline{R}_j = \underline{\mathcal{R}}_j - \underline{r}_j \tag{6}$$

where R_j is the distance between scattering center and detector

$\underline{f}_j(\underline{R}_j,t)$ is the amplitude of the scattered field and is

$$\underline{f}_j(\underline{R}_j,t) = \frac{-4\pi^2}{R_j^3\lambda^2}\,[\underline{R}_j \times (\underline{R}_j \times \epsilon\underline{E}')]\exp[i\omega_o-\gamma)\,t] \tag{7}$$

that is, $\epsilon = \left(\dfrac{e^2\lambda^2}{4\pi^2mc^2}\right)$

$$\underline{f}_j(\underline{R}_j,t) = -\left(\frac{e}{mc^2}\right)\frac{1}{\underline{R}_j}[\hat{\underline{a}}_j \times(\hat{\underline{a}}_j \times \underline{E}')]\exp(i\omega_o t-\gamma t) \tag{8}$$

where $a_j = \dfrac{\underline{R}_j}{|R_j|}$ is the unit vector in the R_j direction r_j is measured from a reference point, 0, in the scattering volume. If the dimensions of the scattering volume are small compared with $\underline{\mathcal{R}}$, then R_j may be replaced by $\mathcal{R}_j$, and

$\underline{f}_j = f$ for all electrons in the plasma volume. When dealing with the phase, however, more care must be taken in approximations. The following substitution may be made for $\underline{r}_j << \underline{R}$.

$$\underline{R}_j = \sqrt{(\underline{R}-\underline{r}_j)^2} = \sqrt{(R^2-2\underline{R}\cdot\underline{r}_j+r_j^2} \approx \frac{R-(\underline{R}'\underline{r}_j)}{R} + \ldots \quad (9)$$

Writing the scattered wave vector k" as having approximately the magnitude of the incident wave vector k' and direction $\underline{R}$, that is,

$$\underline{k}'' = k' \frac{\underline{R}}{|\underline{R}|} \quad (10)$$

(5) may be rewritten as

$$\underline{E}_j''(\underline{R},t) = \underline{f}(\underline{R},t,\lambda\theta)\exp(ik'R + i\underline{k}\cdot\underline{r}_j) \quad (11)$$

where $\underline{k}$ is the scattering vector. That is

$$\underline{k} = \underline{k}''-\underline{k}', \quad k = \left(\frac{4\pi}{\lambda}\right)\sin\frac{\theta}{2}, \quad k' \approx k'' = \frac{2\pi}{\lambda} \quad (12)$$

The scattering angle θ is between $\underline{k}'$ and $\underline{k}''$. The direction is of course determined by the incident laser beam and by the position of the detector.

In 90° scattering,

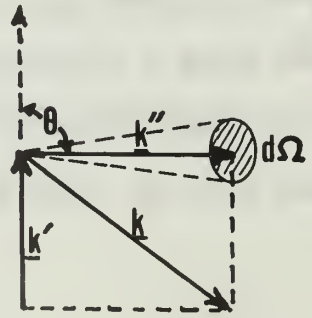

Furthermore $\lambda' \approx \lambda'' = \lambda$. The wavelength difference between λ' and λ'' is usually small and may be neglected, such that the symmetric of the scattered spectrum is undisturbed; if ω_o is the frequency of the incident light and ω is the frequency shift of the scattered light, $I(\omega_o+\omega) \approx I(\omega_o-\omega)$ if no drift velocities exist.

The phase of the scattered light depends on the position of the scattering center by the factor $e^{i\underline{k}\cdot\underline{r}_j}$. This becomes important when the fields scattered by a number of centers are superimposed at $\underline{R}$. Summing, over all electrons in the scattering center, one obtains

$$\underline{E}''(\underline{R},t) = \sum_{j=1}^{N} \underline{E}_j(\underline{R},t) = \underline{f}(\underline{R},t)e^{-ik'R} \sum_{j=1}^{N} e^{i\underline{k}\cdot\underline{r}_j} \qquad (13)$$

The scattered intensity is equal to the time averaged Poynting vector $|\underline{E}''|^2 \frac{c}{4\pi}$; Introducing the incident light intensity as

$$I_o = \frac{|E'|^2 c}{4\pi} \qquad (14)$$

one obtains

$$I(\theta,\lambda) = I(k) = \sigma(\theta) < \left| \sum_{j=1}^{N} e^{i(\underline{k}\cdot\underline{r}_j)} \right|^2 > \qquad (15)$$

Where $\sigma(\theta)$, Thomson's scattering factor, is equal in essence to $|f^2|$; Introducing e' and e", the polarization vectors of the incident and scattered light,

$$\underline{E}' = e'|\underline{E}'| \ , \quad \underline{E}'' = e''|\underline{E}''| \ , \quad \underline{\mathcal{R}}\cdot e'' = 0 \tag{16}$$

$$\sigma(\theta) = \frac{|\underline{f}|^2 c}{4\pi} = I_o \left| e''\cdot (\epsilon e') \frac{4\pi^2}{\lambda^2 \mathcal{R}} \right|^2 \tag{17}$$

for linearly polarized light; and for natural incidents light,

$$\sigma(\theta) = I_o \left(\frac{e^2}{mc^2} \right)^2 \frac{(1 + \cos^2\theta)}{2\mathcal{R}^2} \tag{18}$$

where the 1 in parentheses represents the contribution from natural incident light and $\cos^2\theta$ represents the contributed polarized parallel to the plane of scattering. It is easily seen how (17) complies with this.

B. SPECTRAL INTENSITY DISTRIBUTION OF SCATTERED LIGHT

For the most part, it is the electron density fluctuations in the plasma which are responsible for the scattering of light; that is, according to Huygen's principle no scattering can occur in a strictly homogeneous medium. The electron density $n(\underline{r},t)$ is a function of position and time, and may be considered as a continuously varying quantity or as a superposition of delta functions as circumstances warrant.

Imagine the plasma confined to a large cubical volume $V = L^3$ and write the electron density as a spacial fourier series.[1]

$$n(\underline{r},t) = \frac{1}{V} \sum_{\underline{q}} n_{\underline{q}}(t) e^{i\underline{q}\cdot\underline{r}} \tag{19}$$

Where $\underline{q}$ is the wave vector satisfying the cyclic boundary conditions

$$q_i = \frac{2\pi h_i}{L} \quad h = 0, \pm 1, \pm 2 \quad , \; h_i = x,y,z \tag{20}$$

The fourier coefficient $n_{\underline{q}}$ may be considered as the amplitude of the longitudinal plasma wave with wave vectors $\underline{q}$ and may be written

$$n_{\underline{q}} = \int_V n(\underline{r},t) \exp(-i\underline{q}\cdot\underline{r}) dr \tag{21}$$

for the microscopic representation and

$$n_{\underline{q}} = \sum_{j=1}^{N} \exp(-i\underline{q}\cdot\underline{r}_j) \tag{22}$$

for the microscopic representation.

Usually, longitudinal oscillations in plasmas have complicated time dependencies and dispersion relations; furthermore a number of frequencies may be present. The probability

---

[1] As done in Light Scattering and Drift Instability in a Plasma by Otto Theimer. ltc.

of a certain frequency occurring is related to the mean square of the amplitude $n_{\underline{q}}(\omega)$ of a wave with wave vector $\underline{q}$ and frequency ω. A long lived, relatively undamped oscillation will have a sharp maximum in $n_{\underline{q}}(\omega)$. A continuous function of the frequency $n_{\underline{q}}(\omega)$ is the Fourier transform of $n_{\underline{q}}(t)$ with respect to time and may be written in integral form;

$$n_{\underline{q}}(\omega) = \int_{-\infty}^{\infty} n_{\underline{q}}(t) \exp(-i\omega t)\, dt \tag{23}$$

But the actual density fluctuation is not by itself of primary concern in scattering theory; rather, the amplitude of the polarization waves $\underline{P}_{\underline{q}}(t)$ induced by the incident radiation is of interest. [Not to be confused with the dipole moments of equation (2)]

$$\underline{P}_{\underline{q}}(t) = \epsilon\, n_{\underline{q}}(t)\underline{E}'(t) \tag{24}$$

Where ϵ is given by (7a) and is the polarization of the free electrons. Again, $\underline{E}'(t)$ is the electric field of the incident laser pulse and has the time dependence

$$\begin{aligned} \underline{E}'(t) &= \underline{E}' \exp[(i\omega_o - \gamma)t] , \quad t > 0 \\ \underline{E}'(t) &= 0 \qquad\qquad\qquad\quad , \quad t < 0 \end{aligned} \tag{25}$$

That is, the laser is fired at $t = 0$ and is essentially overafter $\tau = \frac{1}{\gamma}$. Thus it is seen that the polarization waves have a frequency dependence $(\omega_o + \omega)$ the amplitude of

which decreases exponentially with the laser pulse, as $\exp(-\gamma t)$. That scattered light will of course have the same time dependence, and the scattering waves may be identified as a frequency shift in the scattered spectrum.

Thus the finite laser pulse may be attributed (at least mathematically) to the plasma waves and $n_{\underline{q}}(\omega)$ may be written as

$$n_{\underline{q}}(\omega) = \int_0^\infty n_{\underline{q}}(t) \exp\left[-(i\omega + \gamma)t\right]dt \tag{26}$$

Considering the total scattered intensity, the time average value of the function $n_{\underline{k}}(t)$ is taken

$$\left\langle \left| n_{\underline{k}}(t) \right|^2 \right\rangle = \frac{\int_0^\infty \left| n_{\underline{k}}(t) \right|^2 \exp(-2\gamma t)\,dt}{\int_0^\infty \exp(-2\gamma t)\,dt} = 2\gamma \int_{-\infty}^{\infty} \left| n_{\underline{k}}(t) \right|^2 \exp(-2\gamma t)\,dt \tag{27}$$

By Parseval's Theorem [2] from (26) and (27) it follows that

$$\left\langle \left| n_{\underline{k}}(t) \right|^2 \right\rangle = \frac{\gamma}{\pi} \int_{-\infty}^{\infty} \left| n_{\underline{k}}(\omega) \right|^2 d\omega \,. \tag{28}$$

Clearly, additively combining the square of the amplitudes $\left(\frac{\gamma}{\pi}\right) \left| n_{\underline{k}}(\omega) \right|^2$ gives the square of the amplitude $\left\langle \left| n_k(t) \right|^2 \right\rangle$,

---

[2] In Bronstein and La. Semgndjajew, Taschenbuch d. Matematik, Verlag Harri Deutsch, Frankfurt/M., 1965, va5 pp.404-474.

Thus each wave of wave vector $\underline{k}$ and frequency ω contributes to the total scattered intensity by an amount given by

$$I(\omega, \underline{k})d\omega = \sigma(\theta)\left(\frac{\gamma}{\pi}\right)|n_{\underline{k}}(\omega)|^2 d\omega \left[\frac{\text{watts}}{\text{cm}^2}\right] \qquad (29)$$

And as already stated, each frequency shows up as a frequency shift in the scattered spectrum.

So it has been established that each electron becomes Hertz oscillator, when induced to oscillate by the incident light, and itself emits the light which is the scattered radiation. If all electrons oscillate in phase with the incident light, the emitted (scattered) radiation will be coherent in time. If, however, the electrons have completely arbitrary spacial distribution, coherence is destroyed. But electrostatic interaction prevents the electron distribution from ever being completely arbitrary, and it is from partial spacial coherence that so-called collective scattered radiation is observed. The degree or intensity of coherence is dependent on the ratio α between the wavelength and the characteristic Debye shielding length for the plasma. That is,

$$\alpha_s = \frac{\lambda}{4\pi\,\lambda_D \sin\frac{\theta}{2}}\,, \quad \lambda_D = \left(\frac{KTs}{4\pi ne^2}\right)^{\frac{1}{2}}\,, \quad s = i,e \qquad (30)$$

Where λ is the wavelength of the incident light, λ_D is the Debye length and θ the scattering angle. For $\alpha << 1$ scattering is incoherent; for $\alpha >> 1$ spacial coherence

determines the shape of the scattered spectrum. Perhaps a more physical and qualitative (if not mathematically rigorous) understanding may be had of this concept if one imagines the Debye spheres as integral units. Imagine the electrons as tied to the ions they shield. Within the Debye sphere, the electron distribution is arbitrary; that is, incident of wavelength less than the radius of the Debye sphere will oscillate electrons within that sphere in different phases, whereas incident light of wavelength greater than the Debye sphere will oscillate the Debye spheres, and thus all electrons within them in unison, in coherence.

The incoherent scattering spectrum is a direct illustration of the electron velocity distribution, as will now be shown. As the scattering under consideration is incoherent, the effect of a single electron may be looked at. It has been seen that the electric field of light scattered by the j^{th} electron, by equations (7) and (11) is proportional to the phase factor $\exp[i\omega_o t + i\underline{k}\cdot\underline{r}_j]$. Approximating $\underline{r}_j$ by an expression valid for straight line electron paths,

$$\underline{r}_j(t) = \underline{r}_j(0) + \underline{v}_j t \quad , \tag{31}$$

the scattered field has the frequency

$$\omega'' = \omega_o + \underline{k}\cdot\underline{v}_j \tag{32}$$

and the scattered light is Doppler shifted by $\underline{k}\cdot\underline{v}_j = kv_j$ ($k = k''-k'$). The shift is two fold; that is the electron

is a moving source to the scattered light. Thus the total shift is $\underline{k}\cdot\underline{v} = \underline{k}''\cdot\underline{v} - \underline{k}'\cdot\underline{v}$. $F(\underline{v})$ now, is the normalized velocity distribution function with velocity $\underline{v}$ parallel to $\underline{k}$. Corresponding to velocity $\underline{v}$, the frequency is $\omega = kv$; the velocity interval dv correspond to frequency interval $d\omega = kdv$. Thus, the number of electrons with velocity $\underline{v}$ is proportional to the scattered intensity with shift kv. That is,

$$F_e(v) = \frac{kI(kv,\underline{k})}{I(\underline{k})} \tag{33}$$

where $\underline{v}$ is the velocity component parallel to $\underline{k}$, $I(kv,\underline{k})$ is the scattered intensity integrated over all frequencies. Again, this is only valid for $\alpha << 1$.

The topic now turns to the more complicated theory of longitudinal plasma waves. The attempt here is to calculate the mean thermal value of the square of the space time dependent Fourier coefficients $|n_{\underline{k}}(\omega)|^2$. The basic reference for this calculation is the paper by Salpeter.[3] The amplitude squares $|n_{\underline{k}}(\omega)|^2$ will be solutions of the collisionless Boltzmann equation, i.e. the Vlassov equation (See Appendix A for derivation of the Boltzmann equation). The collisionless Boltzmann equation,

$$\frac{\partial f}{\partial t} + \underline{v}\cdot\underline{\nabla}_r f + \frac{f}{m}\cdot\underline{\nabla}_v f = 0 \tag{34a}$$

---

[3] E. E. Salpeter, Phys. Rev 12, 1528 (1960).

is essentially a continuity equation for representative points in electron phase space. The increase in time in the number of electron points in phase space is caused by three factors: (1) The drift in points in position coordinates due to inherent velocity: (2) the drift in points in velocity coordinates due to electric and magnetic forces, and; (3) the spontaneous velocity change without position coordinate due to collisions.

In the purpose of calculating $|n_k(\omega)|^2$ the spacial Fourier coefficient $f_{\underline{q}\underline{v}}(t)$ of the distribution function $f(\underline{r},\underline{v},t)$ is introduced. ($\underline{q}$ is the general wave vector). Corresponding to equation (22),

$$f_{\underline{q}\underline{v}}(t) = \sum_{j}^{(vdv)} \exp[-i\underline{q}\cdot\underline{r}_j(t)] , \tag{34}$$

the sum being taken over those particles with velocities between $\underline{v}+d\underline{v}$. As $d\underline{v} \to 0$, the right hand side has one term if a particle of velocity $\underline{v}$ exists and no term if such a particle does not exist. Thus (34) represents a <u>fine grained</u> distribution function so described because the density has but two values: zero in a vacuum and infinite at the position where a particle is represented by a mathematical point. Clearly, then, an integral over the velocity distribution becomes identical with a sum over all the particles:

$$\int_{-\infty}^{\infty} f_{\underline{q}\underline{v}}(t)\,d\underline{v} = \sum_{j=1}^{N} \exp[i\underline{q}\cdot\underline{r}_j(t)] \tag{35}$$

The number of terms in (34) is equal to the number of particles with velocities in $\underline{v}$ and $\underline{v} + d\underline{v}$. If the physical properties that are influenced only slightly by the microscopic details of the distribution function are calculated and if the course grained (continuous) distribution is independent of spacial position, the number of terms in the sum is the most important aspect of (34), and may be approximated by

$$f_{\underline{q}\underline{v}}(t) = n(\underline{r},t)F(\underline{v}) = \frac{F(\underline{v})}{V} \sum_{\underline{q}} n_{\underline{q}}(t)\exp(i\underline{q}\cdot\underline{r}) \qquad (36)$$

where $F(\underline{v})$ is the normalized coarse grained (continuous) velocity distribution and $n_{\underline{q}}(t)$ is the Fourier coefficient of the particle density given by (21) and (22). As the notation in (36) implies, $F(\underline{v})$ is independent of time. This of course, is valid only if $\Delta F/F$ is small during the time $1/\Delta\omega$ where $\Delta\omega$ is the practical spectral resolution.

Without regard to the coarse or fine-grained structure of $f_{\underline{q}\underline{v}}(t)$, the distribution function may be represented for ions and electrons as a Fourier series:

$$F_s(\underline{r},\underline{v},t) = \frac{1}{V} \sum_{\underline{q}} f_{s\,\underline{q}\underline{v}}(t)\exp(i\underline{q}\cdot\underline{r}), \quad s = i,e \qquad (37)$$

Similarly, for the three terms in the Vlassov equation,

$$\frac{\partial f_s}{\partial t} = \frac{1}{V} \sum_{\underline{q}} \frac{\partial f_{s\underline{q}\underline{v}}(t)}{\partial t} \exp(i\underline{q}\cdot\underline{r}) \qquad (38)$$

and for the second term

$$\underline{v} \cdot \frac{\partial f_s}{\partial r} = \frac{i\underline{v}}{V} \cdot \sum_{\underline{q}} \underline{q} f_{s\underline{q}\underline{v}}(t) \exp(i\underline{q}\cdot\underline{r}) \tag{39}$$

In the third term, only the electrostatic force $e_s\underline{E}(\underline{r},t)$ is considered where e_s is the charge of the particle at $r\cdot\underline{E}(\underline{r},t)$ is written as a Fourier series,

$$\underline{E}(\underline{r},t) = \frac{1}{V} \sum_{\underline{q}} \underline{E}_{\underline{q}}(t) \exp(i\underline{q}\cdot\underline{r}) \tag{40}$$

For $\frac{\partial f}{\partial v}$ equation (36) is used, where $F(\underline{v})$ is the only velocity dependent quantity. The third term then becomes,

$$\frac{\mathcal{F}_s}{m_s} \cdot \frac{\partial f_s}{\partial \underline{v}} = \frac{e_s}{m_s V^2} \sum_{\underline{q}} [\underline{E}_{\underline{q}'} \exp(i\underline{q}'\cdot\underline{r}) \sum_{\underline{q}} n_{s\underline{q}''} \exp(i\underline{q}''\cdot\underline{r})] \cdot \frac{\partial F_s(\underline{v})}{\partial \underline{v}} \tag{41}$$

Combining terms in the double sum for which

$$\underline{q}' + \underline{q}'' = \underline{q} \quad , \quad \underline{q}'' = \underline{q} - \underline{q}' \tag{42}$$

$$\frac{\mathcal{F}_s}{m_s} \cdot \frac{\partial f_s}{\partial \underline{v}} = \frac{e_s}{m_s V^2} \sum_{\underline{q}} \sum_{\underline{q}'} \underline{E}'_{\underline{q}'} n_{s(\underline{q}-\underline{q}')} \exp(i\underline{q}\cdot\underline{r}) \cdot \frac{\partial F_s(\underline{v})}{\partial \underline{v}} \tag{43}$$

$$= \frac{1}{m_s V^2} \sum_{\underline{q}} \underline{F}_{s\underline{q}} \exp(i\underline{q}\cdot\underline{r}) \cdot \frac{\partial F_s(\underline{v})}{\partial v}$$

where

$$\mathcal{F}_{s\underline{q}} = e_s \sum_{\underline{q}'} \underline{E}_{\underline{q}'} \, n_{s(\underline{q}-\underline{q}')} \tag{44}$$

The "Random Phase" approximation is now introduced. The order of magnitude of $n_{\underline{q}}$ follows from (22). Remember that

$$\lim_{N\to\infty} n_o = N >> n_q - \sqrt{N} \tag{45}$$

$n_{\underline{q}}$ is the sum of N positive and negative term with values arbitrarily distributed from zero to one. The probability that the real and imaginary parts of $n_{\underline{q}}$ have the values $\xi_{\underline{q}}$ and $\eta_{\underline{q}}$ respectively is

$$W(\xi_{\underline{q}}, \eta_{\underline{q}}) = \frac{1}{2\pi N} \exp\left[\frac{-(\xi_{\underline{q}} + \eta_{\underline{q}}^2)}{2N}\right] \tag{46}$$

and the mean amplitude square value is

$$\langle | n_{\underline{q}} |^2 \rangle = \int_{-\infty}^{\infty} \int_{-\infty}^{\infty} d\xi_{\underline{q}} d\eta_{\underline{q}} (\xi_{\underline{q}}^2 + \eta_{\underline{q}}^2) W(\xi_{\underline{q}}, \eta_{\underline{q}}) = 2N \tag{47}$$

(46) and (47) explain the importance of (45). E_o that is, q = 0 has no dominating position for the electric field because it has a mean value in a neutral plasma of zero. Thus (44) has one dominating term only.
Writing explicitly,

$$\underline{\mathcal{F}}_{s\underline{q}} = e_s \left[\underline{E}_{\underline{q}} N + \sum_{\underline{q}' \neq \underline{q}} \underline{E}_{\underline{q}'} n_s(\underline{q}-\underline{q}')\right] \tag{48}$$

The "random phase" approximation assumes that the sum can be neglected in comparison to the term $\underline{E}_q N$.[4] Adopting this approximation, equation (33) finally becomes

$$\frac{1}{V}\sum_{\underline{q}} \exp(i\underline{q}\cdot\underline{r})\left[\frac{\partial f_{sq\underline{v}}}{\partial t} + i\underline{v}\cdot\underline{q} f_{sq\underline{v}} + \frac{e_s n_s}{m_s}\underline{E}_{\underline{q}}\cdot\frac{\partial F_s(\underline{v})}{\partial v}\right] = 0 \qquad (49)$$

The Fourier representation is unambiguous, and thus (49) is valid not only for the sum of all general wave numbers $\underline{q}$ but also for every single $\underline{q}$. Writing (49) explicitly for electrons and multiplying by the electron charge e, the equation for the Fourier coefficient $\sigma_{e,\underline{q},\underline{v}}$ corresponding to charge density $\sigma_{e\underline{v}}$:

$$\frac{\partial \sigma_{e\underline{q}\underline{v}}}{\partial t} + i\underline{v}\cdot\underline{q}\,\sigma_{e\underline{q}\underline{v}} + \frac{e^2 n}{m_e}\underline{E}_{\underline{q}}\cdot\frac{\partial F(\underline{v})}{\partial \underline{v}} = 0 \qquad (50)$$

An analytical expression for $\underline{E}$ may be obtained from Poisson's equation

$$\underline{\nabla}\cdot\underline{E} = 4\pi\sigma = 4\pi(\sigma_e+\sigma_i) \qquad (51)$$

Where σ is the charge density created by electrons and ions. As previously done, let

$$\sigma(\underline{r},t) = \frac{1}{V}\sum_{\underline{q}} \sigma_{\underline{q}}(t)\exp(i\underline{q}\cdot\underline{r}) \qquad (52)$$

---

[4] Though the infinite number of terms in the sum makes it by no means really clear that the approximation is allowable.

From (52), (51), and (40)

$$\sum_{\underline{q}} i\underline{q}\cdot\underline{E}_{\underline{q}} = 4\pi \sum_{\underline{q}} \sigma_{\underline{q}} \ , \ \underline{E}_{q} = -4\pi i \sigma_{\underline{q}} \frac{\underline{q}}{q^2} \tag{53}$$

and $\underline{q} = \underline{k}$ (as in equation (12))

$$\frac{\partial \sigma_{ek\underline{v}}}{\partial t} + ikv\, \sigma_{ekv} = i \left(\frac{4\pi n_e^{\ 2}}{m_{ek}} \right) \sigma_k \frac{\partial F_e(\underline{v})}{\partial v} \tag{54}$$

Where v and E are the components of $\underline{v}$ and $\underline{E}$ parallel to $\underline{k}$ (k is along the z axis). The Fourier time transform of σ_{ekv} is needed in the calculation of the spectral distribution; this is written as in equation (20)

$$q_{ekv}(\omega) = \int_o^\infty \sigma_{ekv}(t) \exp[-(i\omega+\gamma)t]dt \tag{55}$$

Integrating over all velocities,

$$\int_{-\infty}^{\infty} \sigma_{ekv}(\omega)\, dv \equiv Q_{ek}(\omega) = \int_o^\infty \sigma_{ek}(t) \exp[-(i\omega+\gamma)t]dt \tag{56}$$

$q_{ek\underline{v}}(\omega)$ satisfies partial differential equation obtained by equating the transform on the right and left of (54). The following integral is needed

$$\int_o^\infty \frac{\partial \sigma_{ekv}}{\partial t} \exp[-(i\omega+\gamma)t]dt = -\sigma_{ekv}(0) + (i\omega+\gamma) q_{ekv}(\omega) \tag{57}$$

This is obtained by integrating by parts and using (55). Notice that the contribution from the upper limit $\sigma_{ekv}(\infty)$ disappears due to $\exp(-\gamma t)$. Using (57) in (54) gives

$$q_{ekv}(\omega)\,(i\omega+\gamma+ikv) = \sigma_{ekv}(0) + i\left(\frac{4\pi n_e^{\,2}}{m_{ek}}\right) Q_k(\omega)\,\frac{\partial F_e(\underline{v})}{\partial \underline{v}} \tag{58}$$

or multiplying by i

$$q_{ekv}(\omega) = \frac{i\sigma_{ekv}(0) - \left(\frac{4\pi n_e^{\,2}}{m_{ek}}\right) Q_k(\omega)\,\frac{\partial F_e(\underline{v})}{\partial \underline{v}}}{-\omega - kv + i\gamma} \tag{59}$$

where

$$Q_k(\omega) = Q_{ek}(\omega) + Q_{ik}(\omega) \tag{60}$$

The charge density for the ions is obtained similarly, that is,

$$q_{ikv}(\omega) = \frac{i\sigma_{ikv}(0) - \left(\frac{4\pi n_e^{\,2}}{m_{ek}}\right) Q_k(\omega)\,\frac{\partial F_i(\underline{v})}{\partial \underline{v}}}{-\omega - kv + i\gamma} \tag{61}$$

and the total charge density

$$q_{\underline{k}\underline{v}}(\omega) = q_{e\underline{k}\underline{v}}(\omega) + q_{i\underline{k}\underline{v}}(\omega) = \frac{i\sigma_{\underline{k}\underline{v}}(0) - \left(\frac{4\pi n_e^{\,2}}{m_{ek}}\right) Q_k(\omega)\left[\frac{1}{m_e}\frac{\partial F_e(\underline{v})}{\partial \underline{v}} + \frac{1}{m_i}\frac{\partial F_i(\underline{v})}{\partial \underline{v}}\right]}{-\omega - kv + i\omega} \tag{62}$$

Integrating (62) over all velocities gives an expression for $Q_k(\omega)$, which may then be introduced into (59) and that

result integrated over all $\underline{v}$. The final result would be the amplitude necessary for scattering $Q_{ek}(\omega) = - en_k(\omega)$. Since the integrals may not be actually evaluated without choosing special velocity distributions, the following function is introduced

$$G_s(\omega) = - \left(\frac{4\pi n_e^2}{m_{sk}} \right) \int_{-\infty}^{\infty} \frac{\partial F_s(v)}{\partial \underline{v}} \frac{d\underline{v}}{-\omega - kv + i\gamma} , \quad s = i,e. \tag{63}$$

Furthermore, corresponding to (35) the velocity integral may be calculated as a sum if $i\sigma_{\underline{k}\underline{v}}(0)$ is chosen as a fine-grained function.

Then, by integration of (62)

$$Q_{\underline{k}}(\omega) = ie \sum_j \frac{\left[\frac{\exp(-ikZ_j)}{-\omega - kv_{ij} + i\gamma} - \frac{\exp(-ikz_j)}{-\omega - k_{eij} + i\gamma} \right]}{1 - G_e(\omega) - G_i(\omega)} \tag{64}$$

Where Z_j, z_j, v_{ij}, v_{ej} are position and velocity components of ions and electrons parallel to $\underline{k}$ at $t = 0$.

Equation (64) may be considered the basic equation of the theory of longitudinal plasma waves. From this equation follow the formulas for scattering, dispersion and drift instabilities.

The next step is to employ the theory of density fluctuations to light scattering in a Plasma. This requires the amplitude squares $| Q_k(\omega) |^2$ and $| Q_{sk}(\omega) |^2$; these represent a time average and a time integral over all microscopic states assumed by the plasma between $t = 0$ and $t = \frac{1}{\gamma}$.

Substituting (64) into (59) and (61) and integrating over all velocities using the same method by which $Q_{\underline{k}}(\omega)$ was obtained, $|Q_{s\underline{k}}(\omega)|^2$ may be calculated.

$$Q_{e\underline{k}}(\omega) = \frac{-ie}{1-G_e(\omega)-G_i(\omega)}\left[(1-G_i(\omega))\sum_j \frac{\exp(-ikz_j)}{-\omega-kv+i\gamma} - G_e(\omega)\sum_j \frac{\exp(-ikz_j)}{-\omega-kv+i\gamma}\right] \tag{65}$$

and

$$Q_{e\underline{k}}(\omega) = \frac{ie}{1-G_e(\omega)-G_i(\omega)}\left[(1-G_e(\omega))\sum_j \frac{\exp(-ikZ_j)}{-\omega-kv+i\gamma} - G_i(\omega)\sum_j \frac{\exp(-ikz_j)}{-\omega-kv+i\gamma}\right] \tag{66}$$

The amplitude squares $|Q_{sk}(\omega)|^2$ contain double sums of the form,

$$\sum_j \frac{\exp(ikz_j}{-\omega-kv_{ej}+i\gamma} = \sum_j \sum_\ell \frac{\exp[ik(z_\ell - z_j)]}{(-\omega-kv_{ej}+i\gamma)(-\omega-kv_{e\ell}+i\gamma)} \tag{67}$$

as well as double products. Ion velocities and positions are indexed by ℓ, whereas electron velocities and positions are indexed by j. Diagonal terms of the left (the single sum) are treated the same as off-diagonal terms. In the double sum, however, the diagonal terms behave differently; that is, the space dependent phase factor vanishes in these terms allowing the replacement of the sum with an integral over the velocity distribution:

$$\sum_{j=1}^{N} \frac{\exp[ik(Z_j - z_j)]}{(-\omega-kv)^2+\gamma^2} = N\int_{-\infty}^{\infty} \frac{F_e(v)\,dv}{(\omega+kv)^2+\gamma^2} \tag{68}$$

Since the denominator of the right hand integral depends only on v_z, the integral is over the one-dimensional

distribution $F_e(v)$, gotten by integrating $F_e(\underline{v})$ over v_x and v_y. Rigorous evaluation of the integral is at best tedious. It may, however, be approximated more readily. The main contribution to the integral comes at resonance $v = -\frac{\omega}{k}$. At resonance, the value of the denominator varies rapidly while the numerator varies slowly, permitting it to come out of the integral.

$$\lim_{\gamma \to 0} \int_{-\infty}^{\infty} \frac{F_e(v)\,dv}{(\omega+kv)^2+\gamma^2} = F_e\left(\frac{-\omega}{k}\right) \int_{-\infty}^{\infty} \frac{dv}{(\omega+kv)^2+\gamma^2} = \frac{\pi F_e(\frac{-\omega}{k})}{\gamma k} \tag{69}$$

yielding an expression for the diagonal sum dependent on the time of observation $\frac{1}{\gamma}$. This, of course, is what is expected, since $|Q_\ell(\omega)|^2$ determines the scattered radiation during $\tau = \frac{1}{\gamma}$.

The off-diagonal terms behave somewhat differently. It will be shown that this sum may be neglected compared with the diagonal terms. The sum is independent of γ and may be neglected in comparison to the double sum (which depends on $\frac{1}{\gamma}$) for small γ. Consider the double sum over a factor $\exp[ik(z_\ell - z_j)]$ and assume the denominator is replaced by an appropriate mean value. The result is a sum over $N(N-1) \simeq N^2$ positive and negative terms. From the same "random phase" the sum is of the order of magnitude N. Hence,

$$\sum_j \sum_{\ell \neq j} \frac{\exp[ik(z_\ell - z_j)]}{(-\omega - kv_{ej} + i\gamma)(-\omega - kv_{e\ell} - i\gamma)} \simeq N \int_{-\infty}^{\infty}\int_{-\infty}^{\infty} \frac{F_e(v_j)F_e(v_\ell)\,dv_j\,dv_\ell}{(-\omega - kv_j + i\gamma)(-\omega - kv_\ell - i\gamma)} \tag{70}$$

The single integrals over dv_j and dv_ℓ have linear resonances, which by symmetry are integrable; the numerator remains unchanged as the denominator changes sign. Thus the resonance contribution to the integral is zero. Therefore the single integrals are independent of γ and may be neglected in comparison to the diagonal terms proportional to $\frac{1}{\gamma}$. One then obtains,

$$\frac{|Q_{ek}(\omega)|^2}{e^2} = |n_k(\omega)|^2 = \frac{\pi N}{\gamma k} \frac{|1-G_i(\omega)|^2 F_e(\frac{-\omega}{k}) + |G_e(\omega)|^2 F_i(\frac{-\omega}{k})}{|1-G_e(\omega)-G_i(\omega)|^2} \tag{71}$$

$$\frac{|Q_{ik}(\omega)|^2}{e^2} = \frac{\pi N}{\gamma k} \frac{|1-G_e(\omega)|^2 F_i(\frac{-\omega}{k}) + |G_i(\omega)|^2 F_e(\frac{-\omega}{k})}{|1-G_e(\omega)-G_i(\omega)|^2} \tag{72}$$

$$\frac{|Q_\ell(\omega)|^2}{e^2} = \frac{\pi N}{\gamma k} \frac{F_e(\frac{-\omega}{k}) + F_i(\frac{-\omega}{k})}{|1-G_e(\omega)-G_i(\omega)|^2} \tag{73}$$

Evaluation of these amplitude squares of course depends on calculating G_e and G_i for special electron and ion velocity distributions.

Of interest is the shifted Maxwellian distribution;

$$F_s(\underline{v}) = \left(\frac{m_s}{\alpha \pi k T_s}\right)^{\frac{3}{4}} \exp\left[-\frac{m_s}{\alpha k T_s}(\underline{v} + W_s)^2\right] \tag{74}$$

where W_s is the drift velocity of particles of type S, (S = i,e)

Clearly,

$$\frac{\partial F_s(\underline{v})}{\partial v} = \left[\frac{m_s}{kT_s} (v + W_s) \right] F_s(\underline{v}) \tag{75}$$

and

$$G_s(\omega) = k\alpha_s^2 \int_{-\infty}^{\infty} \frac{(v+W_s) F_s(v)\, dv}{(-\omega - kv + i\gamma)} \tag{76}$$

where α_s is given by (30) and $G_s(\omega)$ by (63), and where $F_s(v)$ is a one-dimensional velocity distribution in v_z, and W_s is the z component of W_s.

Introducing the Doppler shifted frequency, one has:

$$\omega_{sw} = \omega - kW_s \tag{77}$$

Quantities of the <u>unshifted</u> (no drift velocity) distribution will now be superscripted with a zero.

Then,

$$G_s(\omega) = k\alpha_s^2 \int_{-\infty}^{\infty} \frac{(v+W_s) F_s^0(v+W_s)\, d(v+W_s)}{[-\omega_{sw} - k(v+W_s) + i\gamma]} = G_s^0(\omega_{sw}) \tag{78}$$

and

$$\int_{-\infty}^{\infty} \frac{F_s(v)\, dv}{(\omega + kv)^2 + \gamma^2} = \int_{-\infty}^{\infty} \frac{F_s^0(v+W_s)\, d(v+W_s)}{[\omega_{sw} + k(v+W_s]^2 + \gamma^2} = \frac{\pi}{\gamma k} F_s^0 \left(\frac{-\omega_{sw}}{k} \right) \tag{79}$$

Using the Doppler shifted frequencies

$$\omega_{s,s}^2 = \frac{2}{3} k^2 v_{s,s}^2 = \frac{2\omega_{ps}^2}{\alpha_s^2} \quad , \quad s,s' = i,e \tag{80}$$

where $v_{s,s'}^2$ is the mean thermal velocity square of the particles of mass m_s and temperature T_s, and introducing the dimensionless frequencies

$$x' = \frac{\omega_{ew}}{\omega_{ee}} \qquad y' = \frac{\omega_{iw}}{\omega_{ii}} \tag{81}$$

it follows that (using (74)),

$$|n_k(\omega)|^2 = \frac{N\pi^{\frac{1}{2}}}{\gamma\omega_{ee}} \left[\frac{|1-G_i(y')|^2 \exp(-x'^2) + |G_e(x')|^2 \eta \exp(-y'^2)}{|1-G_e(x') - G_i(y')|^2} \right] \tag{82}$$

and,

$$y' = \frac{\omega}{\omega_{ii}} - \left(\frac{3}{2}\right)^{\frac{1}{2}} \frac{W_i}{v_{ii}} \quad , \quad x' = \frac{\omega}{\omega_{ii}\eta} - \left(\frac{3}{2}\right)^{\frac{1}{2}} \frac{W_e}{\omega_{ee}} \tag{83}$$

where

$$\eta = \left(\frac{T_e}{T_i}\right)^{\frac{1}{2}} \left(\frac{m_e}{m_i}\right)^{\frac{1}{2}} \tag{84}$$

Furthermore, if the substitution

$$u = W + v \tag{85}$$

is made, and the integrand of (79) is expanded with the factor $(-\omega-ku-i\gamma)$, then,

$$G(x) = k\alpha^2 \int_{-\infty}^{\infty} \frac{uF^0(u)(-\omega-ku-i\gamma)\,du}{(-\omega-ku)^2+\gamma^2} \tag{86}$$

The imaginary part is an integral of the form of (69). Therefore,

$$\lim_{\gamma\to 0} I(x) = \pi^{\frac{1}{2}}\,\alpha x \exp(-x^2) \tag{87}$$

Assuming γ small the real part of G(x) may be expanded in a power series, which, when evaluated, is equal to zero in the limit. Using the same arguments as with (70), the real part goes through zero at resonance and changes sign. Again, integrated over symmetric limits, the integral goes to zero.

From $F^0(u)$, let $\langle|u|\rangle$ be the mean value of $|u|$; expanding the integrand of (86) for $\omega > k\langle|u|\rangle$ in the form

$$\lim_{\gamma\to 0} \frac{-\omega-ku}{(-\omega-ku)^2+\gamma^2} = \frac{1}{-\omega-ku} = \frac{-1}{\omega}\sum_{\nu=0}^{\infty}(-1)^{\nu}\left(\frac{ku}{\omega}\right)^{\nu} \tag{88}$$

the following is obtained:

$$\lim_{\gamma\to 0} Re(x) = \frac{\alpha^2}{\alpha x^2}\left(1 + \frac{3}{2}x + \frac{15}{4}x^2 + \cdots\right) \tag{89}$$

For $\omega < k\langle|u|\rangle$, the substitution,

$$\xi = ku - \omega, \quad u = -\frac{(\xi+\omega)}{k}, \quad du = -\frac{d\xi}{k} \tag{90}$$

is made and $F^0(u)$ is expanded. That is,

$$F^0(u)=F^0\left(\frac{\xi+\omega}{k}\right) = F^0\left(-\frac{\xi}{k}\right)\exp(-x^2)\sum_{\nu=0}^{\infty}\frac{(-1)^\nu}{\nu!}\left(\frac{m\omega}{k^2KT}\right)\xi^\nu \tag{91}$$

Using this to obtain

$$\lim_{\gamma\to 0} \mathrm{Re}(x) = -\alpha^2\left[1-2x^2\left(1-\frac{2}{3}x^2+\frac{4}{15}x^2+\cdots\right)\right]= -\alpha^2[1-F(x)] \tag{92}$$

where f(x) is identified with

$$f(x) = \alpha x \exp(-x^2)\int_0^x \exp(t^2)\,dt \tag{93}$$

because this function has the same series expansion. Thus, finally,

$$G_s(x_s') = -\alpha_s{}^2[1-f(x_s')- i\pi^{\frac{1}{2}} x_s' \exp(-x_s'^2)] \quad s=i,e \quad x_i' = y' \tag{94}$$

What has been presented here is the linear theory for scattering. Appendix B gives calculated example curves of spectral distributions of plasmas with drift velocity W (W is smaller than W_{kr}, the critical velocity at which non-linear drift instabilities are excited) W is in multiples of the electron thermal velocity $(\frac{3}{2})^{\frac{1}{2}} v_{ee}$; α is α_e, the

parameter identified in equation (30) and $\epsilon = \frac{T_e}{T_i}$. Each spectrum contains 11 curves[5] from angles $\phi = 0, \frac{\pi}{10}, \frac{2\pi}{10}, \ldots \pi$ between $\underline{W}$ and $\underline{k}$ with $W_z = |\underline{W}| \cos\phi$. The curves with the most pronounced side maxima correspond to $\phi = \frac{\pi}{2}$, the only symmetric curve corresponding to $\phi = \frac{\pi}{2}$ with the horizontal tangent at y = 0. y is of course the dimensionless frequency $\frac{\omega}{\omega_{ii}}$, and extends over $|y| \leq 3.5$ representing the ion line. Relative maximum intensity I_m is given for each, since intensities vary strongly. Intensities are normalized so that

$$I(\omega,k) = \frac{|1-G_i(y)|^2 \exp(-x'^2) + |G_e(x')|^2 \eta \exp(-y^2)}{|1-G_e(x') - G_i(y)|^2} \qquad (95)$$

---

[5] From the report by Theimer; by permission of Professor F. Schwirzke.

III. APPARATUS

The experimental setup itself requires a myriad of equipment. The schematic of figure 1 shows the equipment involved and its layout. The steady-state plasma facility at the Naval Postgraduate School is ideal for a systematic investigation of the laser light scattering plasma diagnostic technique. The parameters of plasma density and electron temperature may be varied over wide range in the system. The plasma, whether argon, nitrogen, or helium, is produced through a hollow tantalum cathode and is accelerated to a disc anode between voltages of around 40 volts. The beam is columnated at the cathode by an arrangement of wound electromagnets producing fields of several hundred gauss. The plasma density may be controlled by varying the gas flow at a needle valve, altering the background pressure with a 10 inch diffusion pump, and by adjusting the field strengths of the columnating electromagnets. Plasma, and hence electron, densities, as seen in the theory, have a direct bearing on the scattered light intensities. Preparation of the system required the construction and placement of perpendicular window ports through which the incident light entered and the scattered light emerged. The ports were approximately a half inch in diameter and were mounted on removable flanges, as shown in figure 6. The plane described by the perpendicular incident and scattered light wave vectors was arranged in such a way as to intersect

the plasma jet at a point within a half inch of the tantalum cathode outlet, for two reasons. One, this is presumably where the beam and hence the electron density are the greatest; secondly, little is known about the plasma parameters at the cathode... the scattering technique should yield much information concerning these parameters. Furthermore, laboratory space limitations and apparatus configuration demanded location at the spot chosen.

The incident laser radiation was provided by the model 130 high peak power Q-switched laser, manufactured by Optics Technology, Inc. The instrument consisted of a power supply/control console and a separate optical head, which incorporated a Fabry-Perot type interferometer and laser cavity mounted on a granite base. The Q-switch is a device which enables the laser to deliver extremely high peak power pulses varying from one to a hundred megawatts. As here employed, it was a bleachable liquid system contained in a small cell with optically flat faces, which only needed to be inserted between the laser ruby and the interferometer for operation. Further function and use of this device will be discussed later. The laser crystal is a production quality, 60^{o} orientation, three-eighth by three inch ruby crystal, emitting radiation at 6943 $\mathring{A}$. The crystal is optically pumped by two linear xenon arc lamps with three inch arc spacing and overall diameter of eleven mm, mounted opposite the crystal holders in a polished aluminum cavity.

Cooling is accomplished through a forced draft, water-cooled air system. The rear element of the Fabry-Perot interferometer is a TIR prism, and a multi-element glass reflector mounted on a micrometer driven assembly comprises the front element. Alignment of the interferometer optics is extremely critical for lasing action to occur. Alignment may be accomplished in the following way. With the top of the laser cavity and the ruby crystal removed, carefully position a cw laser so that its beam is in line with the axis of the ruby crystal holder pins and passing through the center of the exit hole as shown.

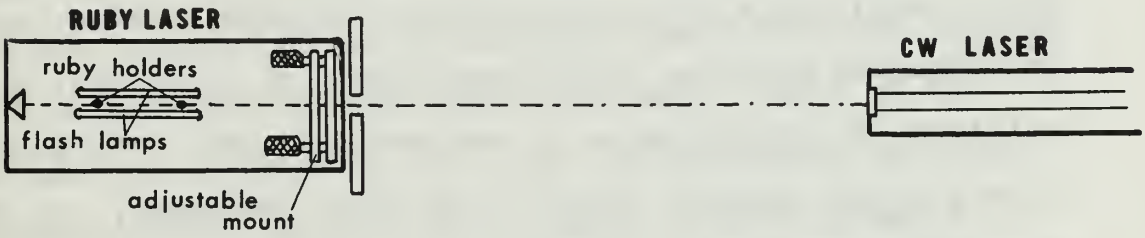

The task of aligning the cw laser may be more easily accomplished accurately by placing a pen or a pencil on the ruby pins, holding it vertically, and adjusting the cw laser until the beam strikes the pencil in the center when placed on either pin. There will now be a multitude of reflections on the face of the cw laser, one from the TIR prism and one from each of the glass reflectors in the micrometer driven interferometer. Determine which one of these reflections comes from the ITR prism by placing a sheet of

paper directly in front of the prism; Once finding the correct reflection, remove the paper and hand adjust the prism until its reflection is as close to the cw exit aperture as possible. Then tighten its screws at its base to secure it. Next adjust the micrometer screws on the interferometer until the multiple reflections made by its elements merge on or near the cw exit aperture and prism reflection. This accomplished, fringe patterns should be observed, and the ruby laser is aligned.

The bleachable dye Q-switch device previously mentioned permits the formation of giant pulses. The technique, usually referred to as passive Q-switching employs a small cell containing a solution of one of several metallo-organic compounds known as phthalocyanines. In this case, a solution of cryptocyanine in methanol is used. The solution strongly absorbs light of the ruby frequency, and this absorption prevents net amplification of light until a greater proportion of Cr^{3+} ions have been pumped into the upper energy state than is normal. The energy input continues until the amplification in the ruby overcomes losses due to absorption in the cell. To this point the laser smits coherent light weakly. A small amount of the light bleaches the cryptocyanine which then becomes nearly perfectly transparent to the ruby light. At the same instant there is a large net amplification and a giant pulse containing all the stored ruby energy develops rapidly.

Following the pulse, the solution returns quickly to its absorbing state. Below is a typical phthalocyanine absorption curve:

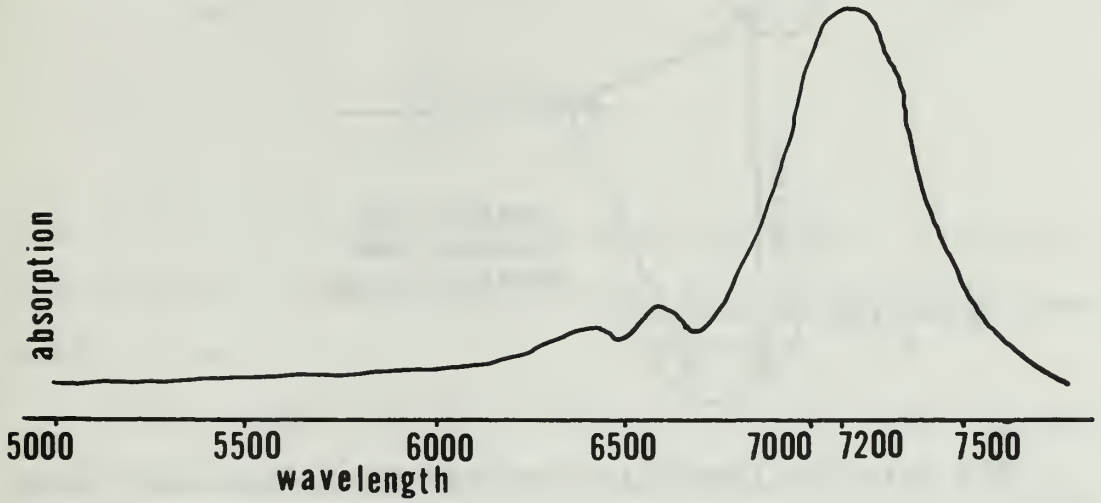

Bleaching of the metal cryptocyanines is effected by the saturation of the absroption at the ruby frequency. That is, the solution is in the bleached condition whrn the population densities in the upper and lower states of the phthalocyanine molecule (S',S in the diagram below) are roughly equal. Because of the large cross-sections for capturing ruby light only small numbers of cryptocyanine molecules are involved. Consequently saturation occurs rapidly and relatively few quanta from the laser beam are required.

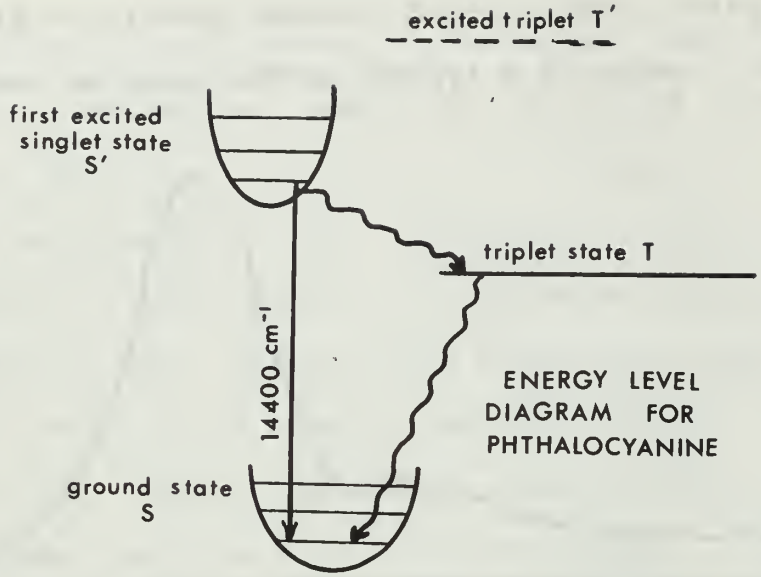

The solution itself is prepared from the concentrate by diluting one part cryptocyanine to ten parts methanol. The cell is filled almost to capacity with methanol and nine drops of the 1:10 solution is added to this. This appears to give optimum Q-switching without requiring too high a threshold.

Calibration of the laser output, that is, determining output energies and pulse widths (and hence output power) involves the use of a PIN photodiode (See Appendix C) and a laser radiometer. The HPA 4205 is a silicon planar PIN photodiode with a response time of less than one nanosecond and a frequency response from dc to 10^9 hz. The diode was wired according to the following diagram.

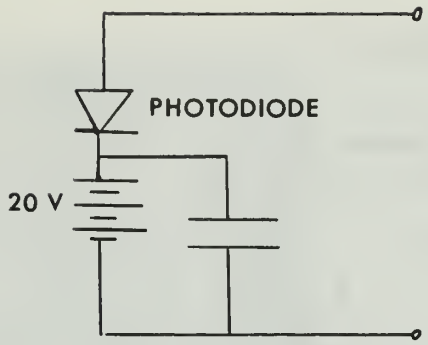

The photodiode is useful in conjunction with a fast-rise oscilloscope, such as a tektronix 519, for recording laser pulse shapes.

Laser output energy was measured using a Westinghouse model RN-1 Radiometer which is, more specifically a calorimetric bolometer. It is designed to trap the energy beam from the laser in a bundle of fine, insulated copper wire which functions both as a calorimetric m ass and as a bolometric element. The change in resistance of the wire element is proportional to the energy absorbed and is almost entirely independent of the distribution of the energy within the unit. The bolometer element is part of a conventional Wheatstone bridge circuit and the change in balance of the bridge is a measure of beam energy. (See figure 4.) When used in conjunction with an electronic microvoltmeter, laser energy may be read directly. When a microvoltmeter reads the imbalance in microvolts, the reading is directly proportioned to the incident laser pulse energy,

$$\left(\begin{array}{c}\text{observed reading} \\ \text{in microvolts}\end{array}\right) \quad \left(\frac{1}{625}\right) = \text{Laser output in joules} \tag{94}$$

The schematic of the calibration setup is as follows:

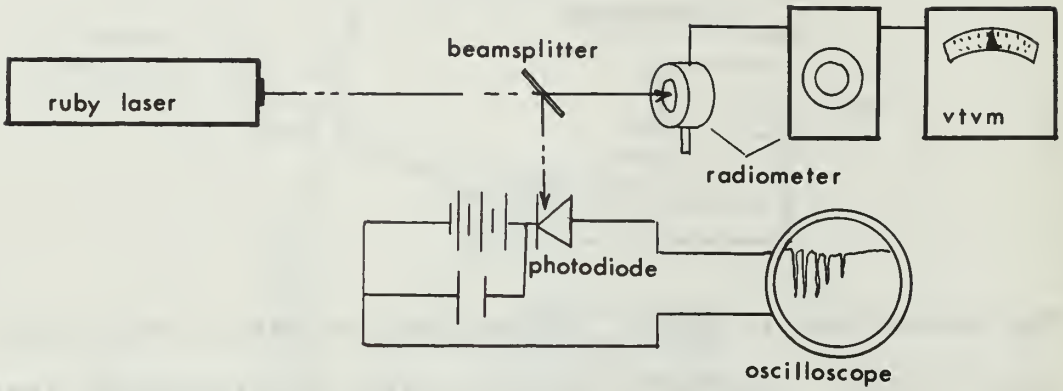

The following are photographs taken on a Tektronix 545A oscilloscope set to trigger as the pulse was initiated. The time scale on the three non Q-switched photos was 50μ s/div., and on the fourth, Q switched pulse 500 ns/div. or 0.5μs/div. This gives an idea of the effectiveness of increasing lasing power by greatly shortening the pulse width. The Q-switched pulse width appears to be of the order of 200ns. The average pulse length of the non Q-switched pulse appears to be of the order of 250μs. Since power is energy per unit time, this shows an increase in lasing power by a factor of 1250. More specifically, a typical low power pulse will put out approximately 0.5 joules. For a pulse width of 250μs this comes out to two kilowatts. The Q-switched pulse width of 0.2μsec. the power is now 2.5 megawatts, a substantial increase. The first three photographs show 3 pulses each; below them is recorded the average energy output of the three for a given input energy from the laser power pack. This was the same for each trace on a given photograph.

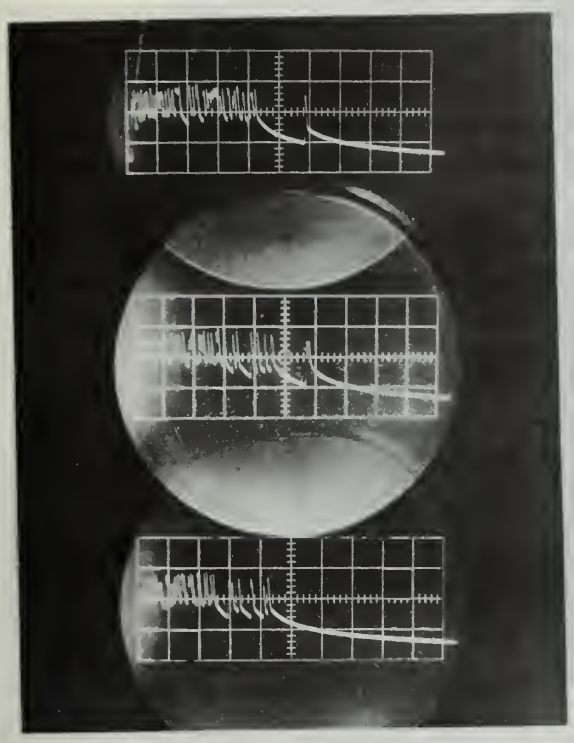

Non Q-Switched Pulses
Sweep Speed = 50 μs/div.

Input 1100 joules
Output 0.19 joules

Input 1225 joules
Output 0.38 joules

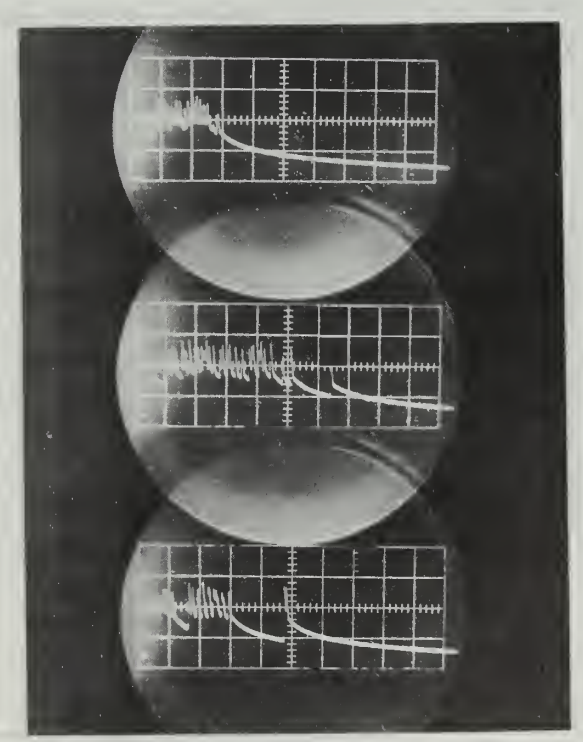

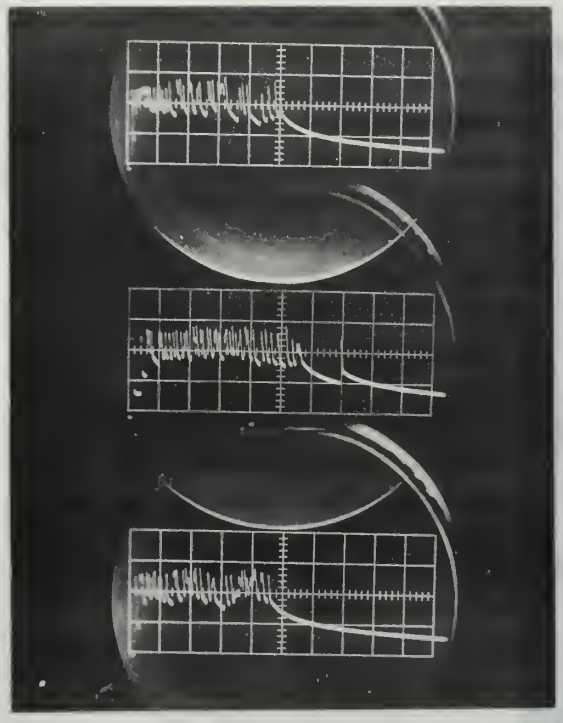

Non-Q-Switched
Sweep Speed 50 μs/div.

Input 1300 joules
Output 0.55 joules

For these first 3 photos, a plot of input versus output energy is made, establishing a linear relationship above laser threshold.

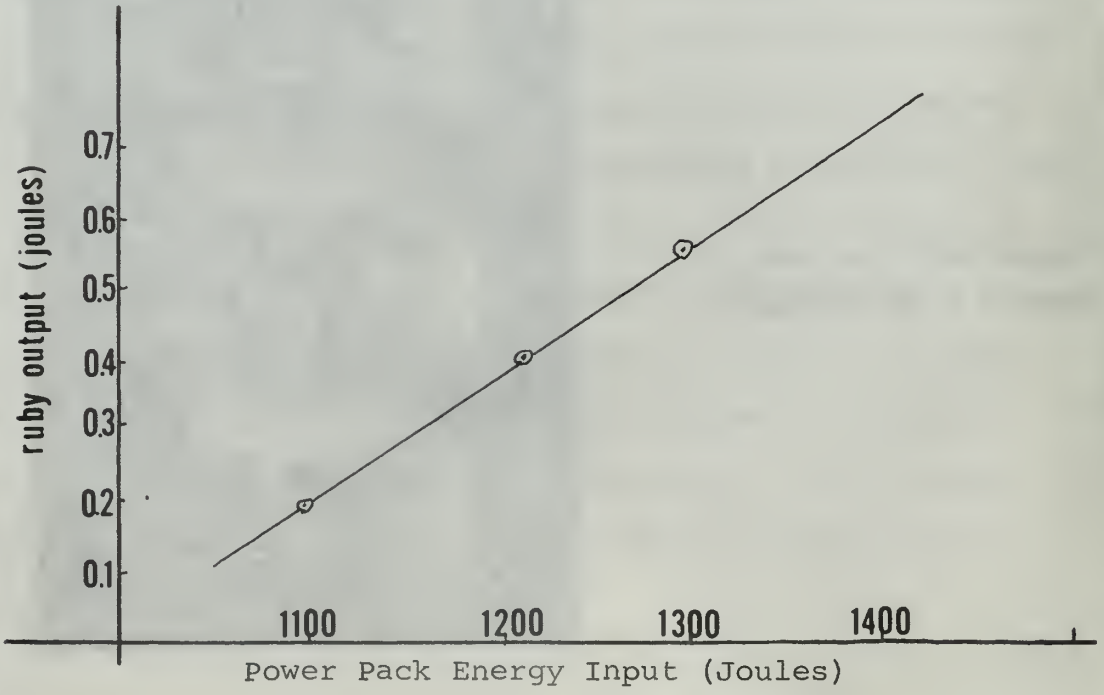

The fourth photo is included as a fine example of a Q-switched laser pulse. Sweeptime here is 0.5 μs/division.

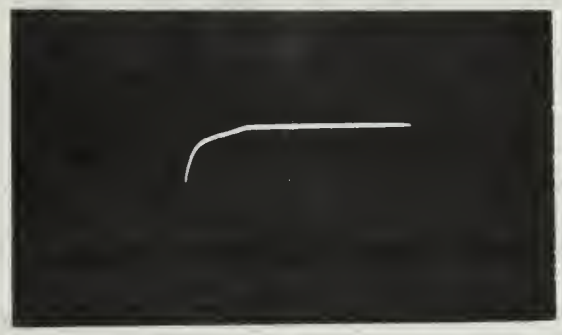

The scattered light is analyzed with the Baird atomic modified Eagle Mount three meter concave Grating Spectrograph. The spectrograph is a Rowland circle type mounting for which the focusing conditions are:

r = RcosA

r'= RcosB

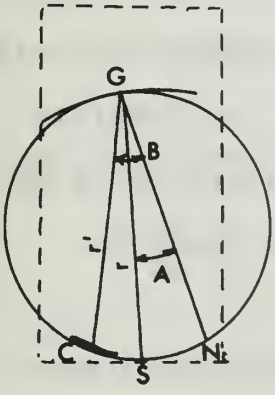

A = Angle of incidence

B = Angle of diffraction

r = Slit to grating distance

r' = Camera to grating distance

R = Radius of curvature of the concave grating.

N = Normal

G = Grating

S = Slit

C = Camera

The Rowland circle has a diameter equal to the radius of curvature of the grating blank. The grating is mounted tangent to the Rowland circle.

The usual grating equation applies. That is

$$n\lambda = d(\sin A + \sin B) \tag{95}$$

n = Order number

λ = Wavelength in Angstroms

d = Grating spacing in Angstroms

A and B are of opposite sign if they are on different sides of the normal. Spectrograph controls include toggle switches for the grating, the plateholder (on which the photomultiplier tubes are mounted) and focus.

Rotating the grating changes the angle of incidence A (and hence B). The Veeder-Root counter is geared so as to indicate the angle of incidence, subtract from 1000. The focus toggle increases or decreases the plateholder to grating distance, the tilt control moves the plate (mounting the photomultipliers) in and out about a vertical axis through the center of the slit. The latter two controls are not as important when using the photomultiplier as opposed to a photographic plate when a careful focus is required.

There existed no calibration chart of the instrument to predetermine the position of the photomultipliers for a specific wavelength. This must be accomplished experimentally, using a calibration source of known wavelength, for

example a helium lamp. Helium has two lines close to the 6943 A ruby wavelength, one at 6730 A and another at 7108 A. Sighting visually through the plate aperture, these may be readily identified. With a slit cut in dark cardboard, the position at which these lines strike the aperture may be marked. Linearly interpolating between the two wavelengths gives a rough position for placement of the photo multiplier. A fine adjustment may be made when the whole system is aligned. The alignment procedure will be described shortly. For purposes of this experiment the proper grating setting was found to be 991.2 (that is, with the angle of incidence A equal to 8.8 degrees.). The dispersion may also be calculated with some ease. This will become of great use when actual spectral distributions are analyzed carefully. This relation may be derived from the basic grating equation.

$$n\lambda = d(\sin A + \sin B) \tag{95}$$

$$\lambda = \frac{d}{n}(\sin A + \sin B)$$

letting d be a constant

$$\left(\frac{\partial \lambda}{\partial B}\right)_d = \frac{d}{n} \cos B \tag{96}$$

or with A constant

$$\frac{d\lambda}{dB} = \frac{d}{n} \cos B$$

$$d\ell = rdB \tag{97}$$

where r is the focal distance and $d\ell$ is the increment along circumference for dB increment.

$$\frac{dB}{d\ell} = \frac{1}{r} \tag{98}$$

$$\frac{d\lambda}{d\ell} = \frac{d\lambda}{dB} \cdot \frac{dB}{d\ell}$$

$$\frac{d\lambda}{d\ell} = \frac{d}{n} \cos B \cdot \frac{1}{r} \tag{99}$$

but

$$r = R \cos B \tag{100}$$

hence $\frac{d\lambda}{d\ell} = \frac{d}{nR} \frac{\cos B}{\cos B}$

D = actual grating spacing.

d = effective grating spacing.

$$\frac{d\lambda}{d\ell} = \frac{d}{nR} \tag{101}$$

$$d = D \cos B \tag{102}$$

therefore

$$\frac{d\lambda}{d\ell} = \frac{D \cos B}{nR} \tag{103}$$

Numerical calculations for dispersion may now be made, letting D be the spacing for 15000 groove/inch grating and R = 3 meters at the 6943A° wavelength and an angle of incidence A (determined experimentally) of 8.8°.

$$D = \frac{1}{15000} \text{ inches} \times \frac{254\text{mm}}{\text{inch}} \times \frac{10^{8}\text{Å}}{\text{cm}} = 16933\text{Å}$$

for the first order spectra

$$\lambda = d(\sin A + \sin B) \qquad A = 8.8^{\circ}$$

$$\sin B = \frac{\lambda}{d} - \sin A$$

$$= \frac{6943}{16933} - \sin 8.8^{\circ}$$

$$= .41003 - .15299$$

$$= .25704$$

$$\therefore \cos B = .96638$$

$$\frac{d\lambda}{d\ell} = \frac{D \cos B}{R} = \frac{(16933)(.96638)}{3 \times 10^{3}}$$

$$= \frac{16369}{3 \times 10^{3}} = 5.45 \text{ Å/mm}$$

The photomultiplier tubes were RCA 7102 tubes with sensitivity and response curves given below.

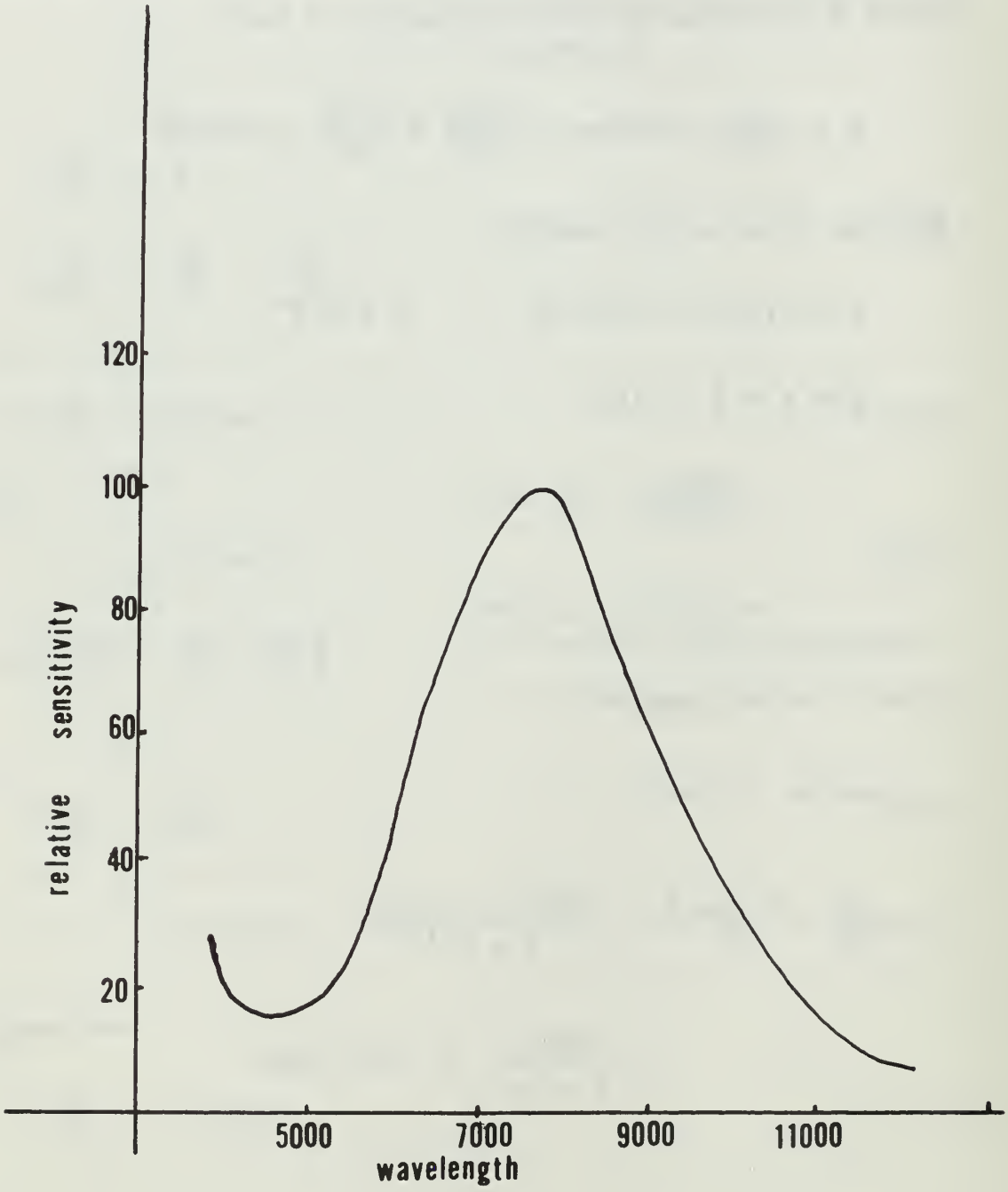

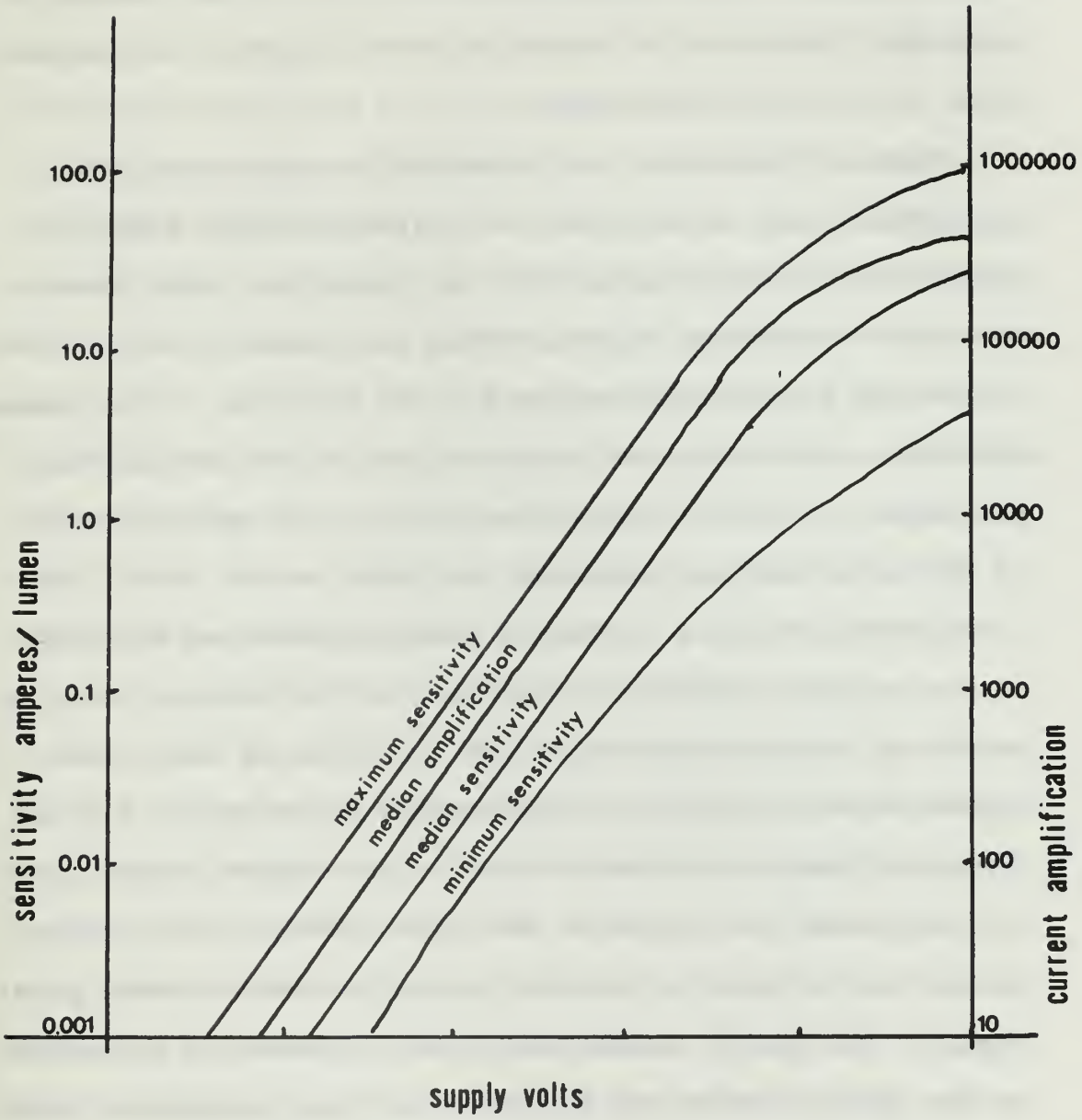

The tubes were operated from a number of power supplies, the best of which appeared to be the Power Designs Model HV 1565 regulated dc power supply. Optimum signal to boise ratio was obtained at a voltage setting between 1450-1490 volts (actual voltage as read on the voltmeter was closer to 1350 volts). The output signal was read

across about a five megohm impedance for greater signal strength. This was of course at some sacrifice to response time, as will be seen later.

Before discussing the important alignment procedure, the optics used to transfer the scattered light from the plasma to the spectrograph will be described. The arrangement was a periscope type as shown in figures 1 and 5. Two converging lenses were employed, one focusing at the plasma, the other refocusing the plasma light at the exit of the periscope. A quartz condensing lens on the optical bench of the spectrograph refocused the light on the slit. An arrangement of rigid cardboard packing tubes and aluminum mirror holders formed the remainder of the device. The position of the periscope exit (on the plane of which the plasma beam is focused) is determined by using the grating lamps and quartz condensing lens in the following way. The grating lamps are hung over the front face of the grating holder and switched on from a control on the external power supply. The quartz condensing lens is placed in its holder on the optical bench and left free to move along the length of the bench. The image of the grating lamps may be observed by holding a white sheet of paper behind the lens. Moving the paper away from the lens will eventually focus the grating lamps in two distinct images. Moving the paper further away, the images will merge, and it is at that

point that the source, in this case the exit of the periscope, is to be placed. The lense is now secured and the periscope is mounted in its proper position.

Because of the distance it was necessary to convey the lights and because of the small image of the lenses, alignment was extremely critical and somewhat difficult to obtain. Accurate laser-plasma-periscope-spectrograph alignment may be obtained while the plasma system is at atmospheric pressure and the tantalum cathodes are being replaced. With the cathode flange removed, remove also the left window flange. Place a wooden slate across two stationary bolts of the cathode flange in such a way as to have the slat horizontal and just below the center of the vacuum chamber (and hence below the plasma beam axis). The carefully insert a rigid aluminum or stainless steel rod down the chamber, supporting one end inside the annular disk anode and the other end on the wooden slat. The slat should be of such thickness that the axis of the rod it supports is parallel to and just below the chamber axis. This arrangement will now support the mirror proble to be inserted from the left window opening; the probe will act as an artificial "scatterer" so that proper alignment both of the optical transfer system and of the grating may be obtained. The mirror probe consists of a straight wooden dowel with one end cut to 45°. To the 45° cut is applied

a small cutout piece of polished stainless steel to act as a reflector. This may be glued on and a mark may then be made on the opposite end of the dowel to indicate the proper vertical mirror position. The dowel is then inserted, one end supported on the rod arrangement described above and the other end on a notched cardboard edge, taped to the window opening. The supporting rod may vary the position of the reflector along the chamber axis without significantly changing its position perpendicular to the axis; pushing or pulling the mirror rod itself, varies its position perpendicular to the chamber axis.

The next step is to place a strong light source such as a mercury lamp before the grating (inside the spectograph) and aimed back toward the slit. The Mercury beam maybe focused at the slit using its own lens for more intensity. With the laboratory darkened, carefully adjust the periscope arrangement until the light from the Mercury falls on the supporting rod, which has been located parallel to the vacuum chamber center axis. This done, the mirror prop may be adjusted so that the light falls on its reflector. From the end of the mirror proble, and peering into the chamber through the left window mount the probe may be adjusted carefully so that its light falls on the half inch laser window. The axis of the mirror should be vertical, that is, reflecting straight up. With the Mercury light, (which may be easily discerned) shining on the half inch laser entrance window, the system, save the laser, should

now be in perfect alignment. The next problem is to align the laser so that its artificially "scattered" light may be seen by the grating; and when this is done the grating must be rotated until the laser frequency is centered on photomultiplier tubes at the spectrograph exit.

The laser is mounted on an aluminum vertically adjustable stand, the laser itself containing tilt adjustment on its base. Alignment along the horizontal plane may be made more easily with a cw laser by raising the axis of the cw laser, the pulse laser may replace along the same axis and trial and error adjustment made until alignment in the vertical plane is achieved at will. Once aligned the laser pulse should be seen in the slit when fired.

The grating may then be rotated to the proper wavelength. The phototubes and grating have already been roughly adjusted according to the helium line procedure described above. First the PIN photodiode is positioned with an arrangement of beamsplitters (microscope slides) to analyze the laser pulse. The signal from the PIN photodiode is then fed to the upper trace of a dual beam oscilloscope, and the signal from the photomultiplier to the lower trace. Upper trace gain is lowered because of the intensity of the laser pulse, but the oscilloscope arrangement is as shown in figure 14. The grating is rotated by 0.1 degree at a time in order to find the optimum position. Below are the traces illustrating how this was accomplished. The upper trace is

the pm tube signal and the lower trace is the laser pulse. Beside each is the respective grating setting and its corresponding angle of incidence.

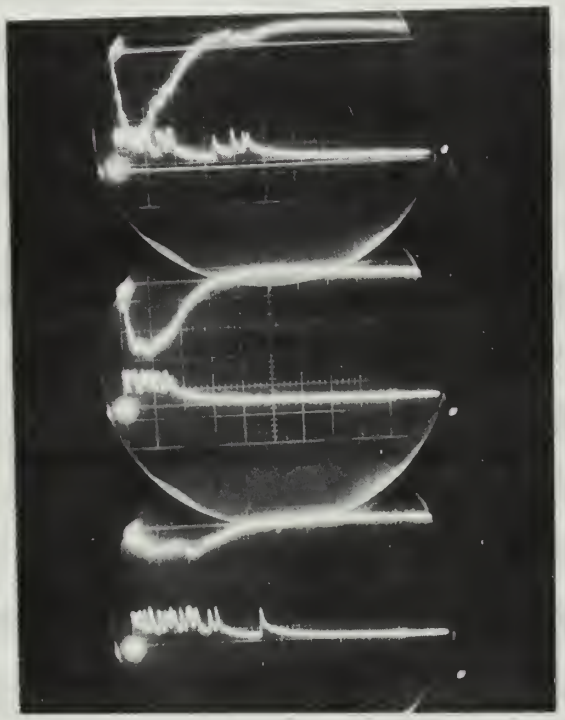

991.2 (8.8°)

991.1 (8.9°)

991.0 (9.0°)

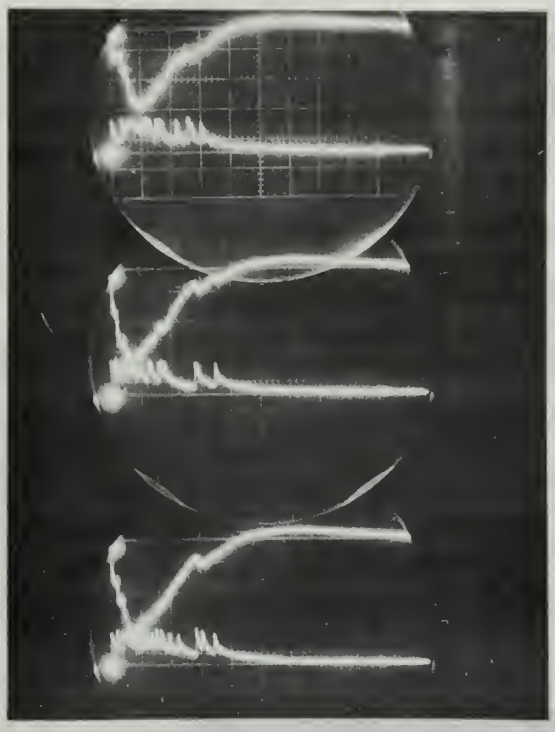

991.5 (8.8°)

991.3 (8.7°)

991.2 (8.8°)

Sweepspeed was 50 μs/div. Both traces were triggered by the laser pulse, the lower trace of each group. The laser trace gain was 0.5 V/div. and the pm tube trace 25 V/div. All were non Q-switched pulses. Note the difference in pulse shapes. As was mentioned before, this was due to

the large resistor in the signal line (about five megohms) which considerably lengthened the rise time of the tubes. This of course, is no consequence since relative intensities are what is important here and in analyzing the spectral distribution of the scattered light.

The system, now constructed and aligned, may be employed in the attempt to discern a scattered light signal and analyze the spectral distribution of the scattered light. The few attempts thus far have been unsuccessful. Some combinations of detecting tubes and oscilloscope amplifiers have been tried to increase the signal to noise ratio. Photographs have been taken, an example of which is below.

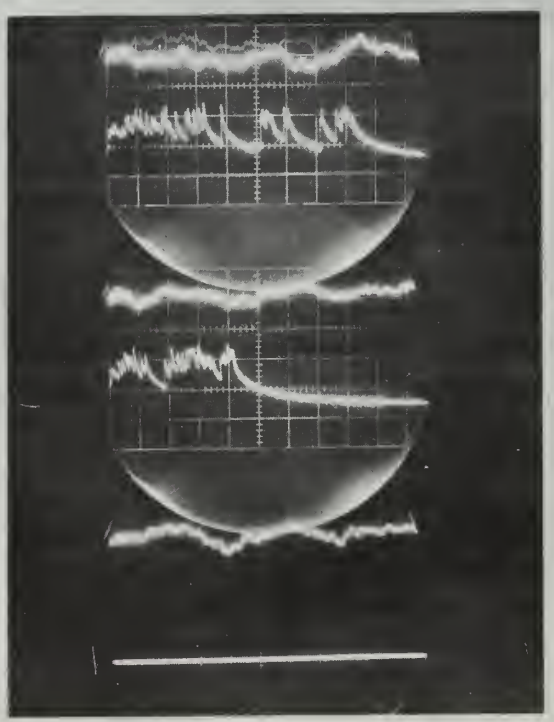

The photograph on the bottom was triggered at the scope with no laser pulse in order to provide a noise reference from the pm tube. Tube voltage was set at 1490 (Actually 1390 on the voltmeter). Sweep speed was 50 μs/div. and the background pressure in the vacuum chamber was 8×10^{-3} mm Hg. Oscilloscope gain here was 0.05 volts/div., as shown in figure 14. If a signal is present, as a few of the traces such as the one above seem to indicate, it is virutally impossible to distinguish it from the noise. Possible improvements will be discussed in the conclusion.

Attempts at focusing the laser beam seem to have no effect, but this is almost certainly due to the poor quality of lenses available.

IV. CONCLUSIONS

The scattering apparatus has been erected and aligned. The attempts which have thus far been made, to discern the scattered light and analyze its spectrum have been unsuccessful. The plasma parameters specifically the density, affect scattering intensities as much as many varied instrument parameters affect the experimenter's ability to detect the light. All oscilloscopes, save a very few are in dire need of realignment and recalibration, as are the plug-in units that accompany them. When the scattered light is finally detected up to seven photomultipliers will be needed to simultaneously analyze the spectral distribution of a single pulse; knowing the dispersion of the grating, the photomultipliers, connected to the spectrograph plate with short lengths pipe, may be accurately spaced around the central frequency to observe the whole spectral distribution of the scattered pulse. These should be of the RCA 7102 type. The 7102 tubes now available appear to have lower signal to noise ratios at sensitivities required that one would expect. Improvement of that ratio could be of significant importance in detecting the scattered light. Increasing the plasma density by purging more gas into the plasma system, increasing the field on the cathode and anode magnets and by controlling the main diffusion pump may well be the answer sought. Furthermore, the laser system available,

while powerful, may not be quite what is needed, though focusing of its beam through a lens of better quality may help. A more energetic system is now on order. It is interesting to note previous experimental attempts to study at light scattering and the problems mentioned in these efforts. One group, Thompson and Fiocco at MIT measure the light of a laser scattered from an electron beam. The electron density was about 5×10^{9} cm^{-3}, and the ratio of scattered to incident intensity was of the order of 10^{-18}! Applying their technique to a low electron density plasma, $n \approx 10^{13}$ cm^{-3}, they improved the ratio of scattered to incident power to 10^{-15}.

The best scattered to incident ratio came from E. Funfer, B. Kronast, and H. J. Kunze, who measured light scattered from a high density pinch plasma ($n \approx 10^{17}$). Their ratio came to 10^{-11}.

Distinguishing the scattered light from background plasma radiation is a considerable problem. One possible solution that may be tried is to eliminate the plasma radiation with polarizers, since at 90^{o} the scattered light will be polarized, whereas the plasma background radiation will not. One other wasy of eliminating plasma radiation would be with the use of a differential amplifier which will differentiate the scattered signal from a pair of pm tubes one seeing the scattered light and radiation, the other only radiation. This technique was attempted, but the characteristics of the two pm tubes available were not close enough

for comparison. Furthermore, the differential amplifier plug-in units on the oscilloscopes were not functioning properly.

The above has summarized experimental progress to date. This progress should enable future experimenters to resume development of the experimental technique of laser light scattering as a plasma diagnostic.

APPENDIX A. DERIVATION OF THE BOLTZMANN EQUATION[6]

Each electron is represented by a point in six dimensional electron phase space. The coordinates of the phase space are x, y, z, u_x, u_y, u_z. Because each electron has a velocity, the representative point for each electron must change its position coordinates with time. In addition, any change in the velocity of the electron will also cause the representative point to move in electron phase space. The velocity of an electron will change if a force acts on the electron or if the electron collides with any other particle.

Consider a fixed differential volume in electron phase space $dV = dx\, dy\, dz\, du\, du_y\, du_z$ (the "electron" subscript will be omitted). An expression will be written for the number of representative points in this volume as a function of r, u, and t; that is, it will be a "continuity" equation for the representative points in electron phase space. The increase with time in the number of electron "points" in dV, $\frac{\partial(f_e dV)}{\partial t}$ is caused by three factors:

1. The drift of points in position coordinates due to inherent velocity.

2. The drift of points in velocity coordinates due to electric and magnetic forces.

---

[6] From Uman, p.34-36.

3. The spontaneous velocity change without position coordinate change due to collisions.

When these three terms are evaluated, the Boltzmann equation for electrons may be written. Note that the effects of external gravitational forces and inteparticle nuclear forces are omitted.

First determined is the increase with time of the number of representative points in dV due to drift in position coordinate space. The number of representative points which cross the surfaces of dV in time $d\epsilon$ because of inherent velocity must be calculated. The velocity of a point in the x direction at x, y, z, u, u_y, u_z is u_x. The number of representative points in a volume of "base area" dy dz du_x du_y du_z and height $u_x dt$ will enter dV in time $d\epsilon$ through a face normal to the x axis at x, y, z, u_x, u_y, u_z. This number is

$$\left[\frac{\partial(d^6N)}{\partial t} \right]_x dt = f_e(\underline{r},\underline{u},t) u_x dt dy dz du_x du_y du_z \qquad (1)$$

The change in the number of representative points in dV in time dt due to the exit of points through the equivalent surface at x+dx is given by

$$\left[\frac{\partial(d^6N)}{\partial t} \right]_{x+dx} dt = - \left[f_e u_x + \frac{\partial(f_e u_x)}{\partial x} dx \right] dt \, dy dz du_x du_y du_z \qquad (2)$$

Therefore the net rate of change of points in dV due to velocity in the x direction is

$$\left[\frac{\partial(d^6N)}{\partial t} \right]_x + \left[\frac{\partial(d^6N)}{\partial t} \right]_{x+dx} = - \frac{\partial(u_x f_e)}{\partial x} \, dV \qquad (3)$$

Thus the total rate of change of points in dV due to inherent velocity may be written as

$$\left[\frac{\partial(d^6N)}{\partial t} \right]_r = - (\underline{u}_e \cdot \nabla r f_e) \, dV \qquad (4)$$

Now consider the drift of representative points in velocity coordinates due to electric and magnetic forces. The "velocity" of a representative point in the u_x direction in velocity coordinates is $\left(\frac{du_x}{dt} \right) = \left(\frac{F_{ex}}{m_e} \right)$. Using this "velocity" the net influx of points through the two surfaces perpendicular to u_x may be calculated:

$$\left[\frac{\partial(d^6N)}{\partial t} \right]_{ux} + \left[\frac{\partial(d^6N)}{\partial t} \right)_{ux+du_x} = - \left[\frac{\partial}{\partial u_x} \left(\frac{F_{ex}}{m_e} f_e \right) \right] dV \qquad (5)$$

The extension of this expression to include the flow through the surfaces perpendicular to u_y and u_z follow

$$\left[\frac{\partial(d^6N)}{\partial t} \right]_u = - \left(\frac{\underline{F}_e}{m_e} \cdot \nabla u \, f_e \right) dV \qquad (6)$$

At this point, the time rate of increase of representative points in dV is equated to the influx from the two drifts (neglecting collisions) and the Boltzmann equation is obtained:

$$\left(\frac{\partial f_e}{\partial t}\right) dV = -\left(\underline{u}_e \cdot \nabla r f_e\right) dV - \left(\frac{\underline{F}_e}{m_e} \cdot \nabla u f_e\right) dV$$

or (7)

$$\frac{\partial f_e}{\partial t} + \underline{u}_e \cdot \nabla r f_e + \frac{\underline{F}_e}{m_e} \cdot \nabla u f_e = 0$$

APPENDIX B

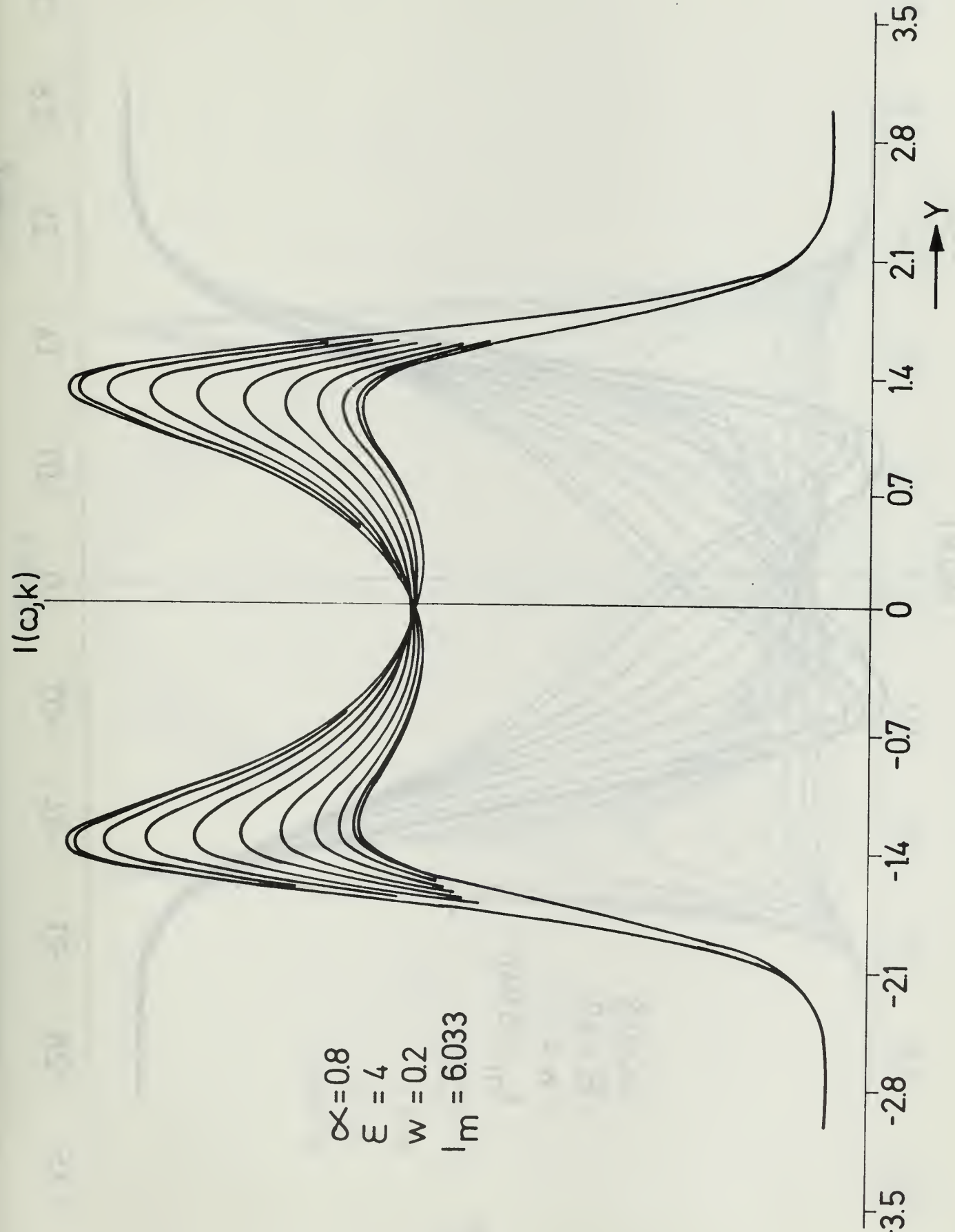

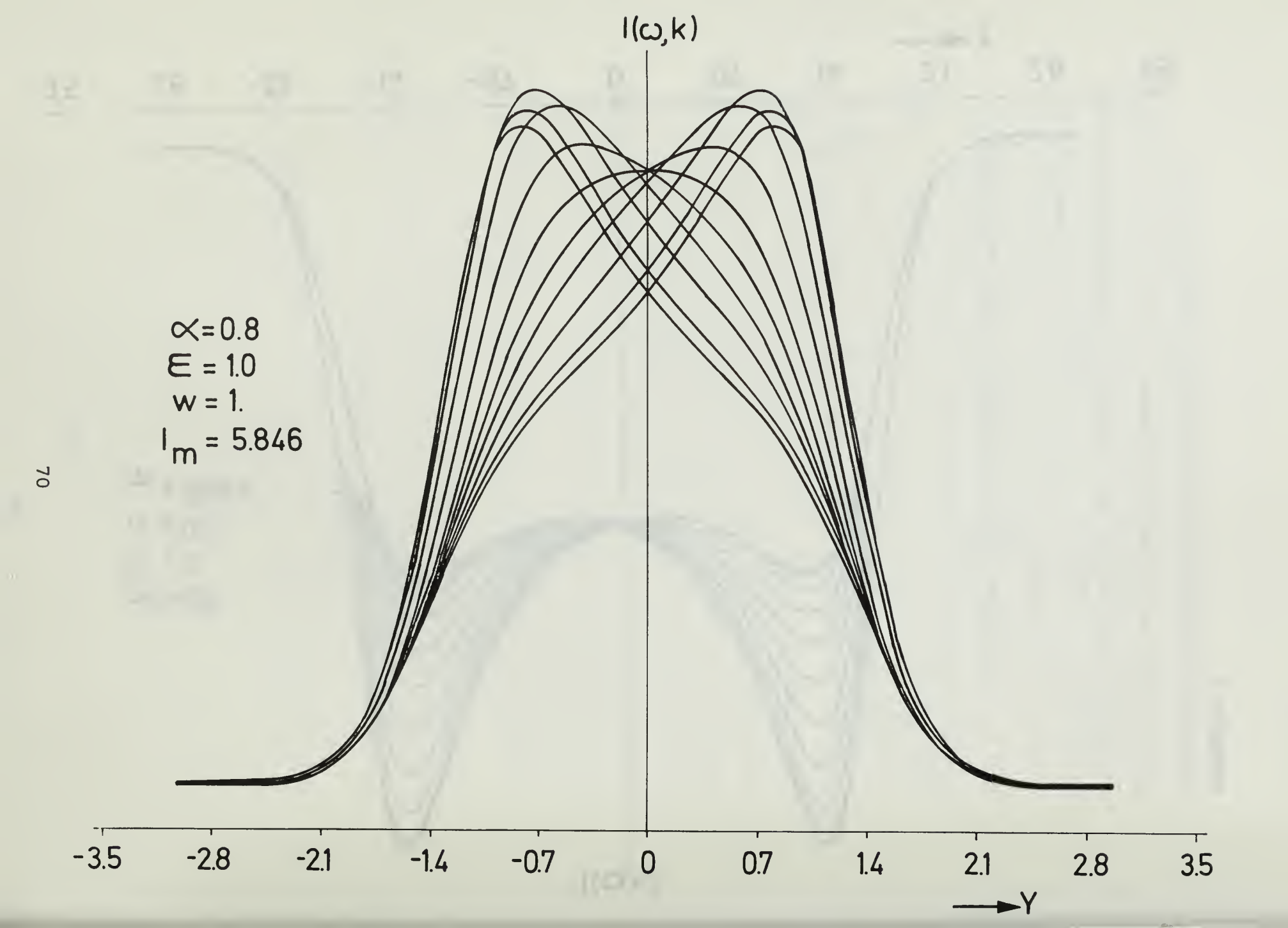
I(ω,k)
∝=0.8
∈ = 1.0
w = 1.
I_m = 5.846
-3.5
-2.8
-2.1
-1.4
-0.7
0
0.7
1.4
2.1
2.8
3.5
Y

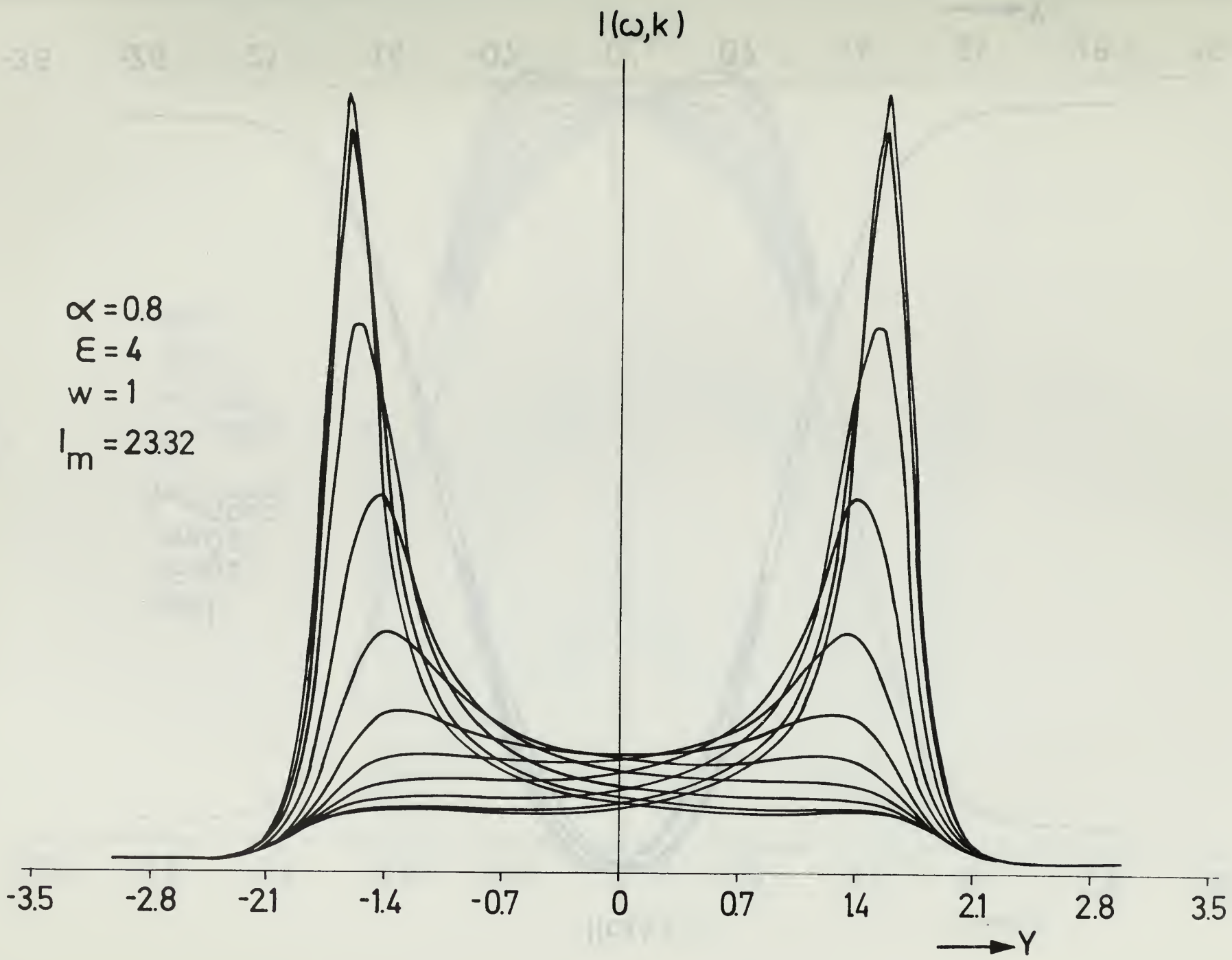
I(ω,k)
α = 0.8
ε = 4
w = 1
I_m = 23.32
-3.5
-2.8
-2.1
-1.4
-0.7
0
0.7
1.4
2.1
2.8
3.5
Y

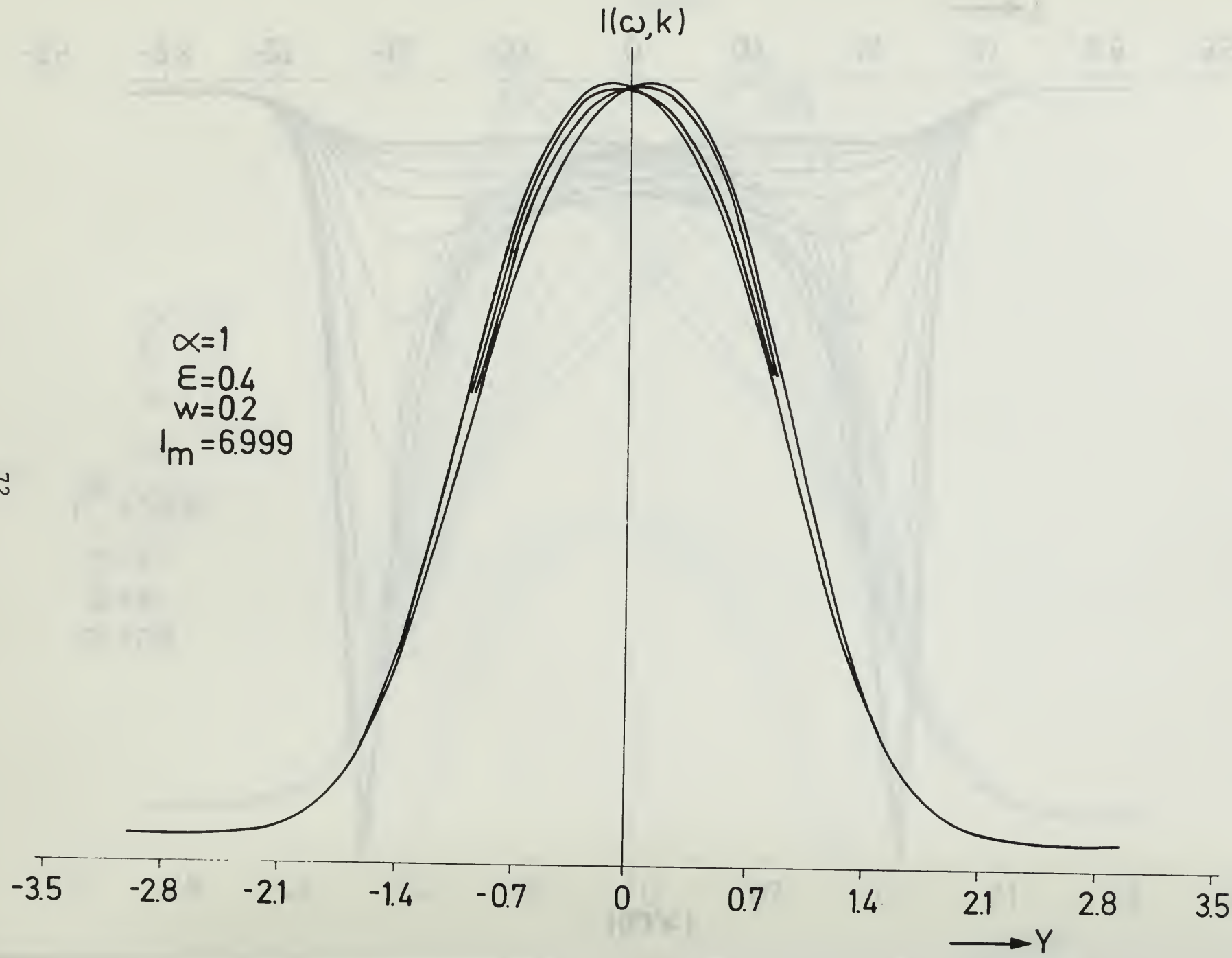
I(ω,k)
∝=1
ε=0.4
w=0.2
I_m=6.999
-3.5
-2.8
-2.1
-1.4
-0.7
0
0.7
1.4
2.1
2.8
3.5
Y

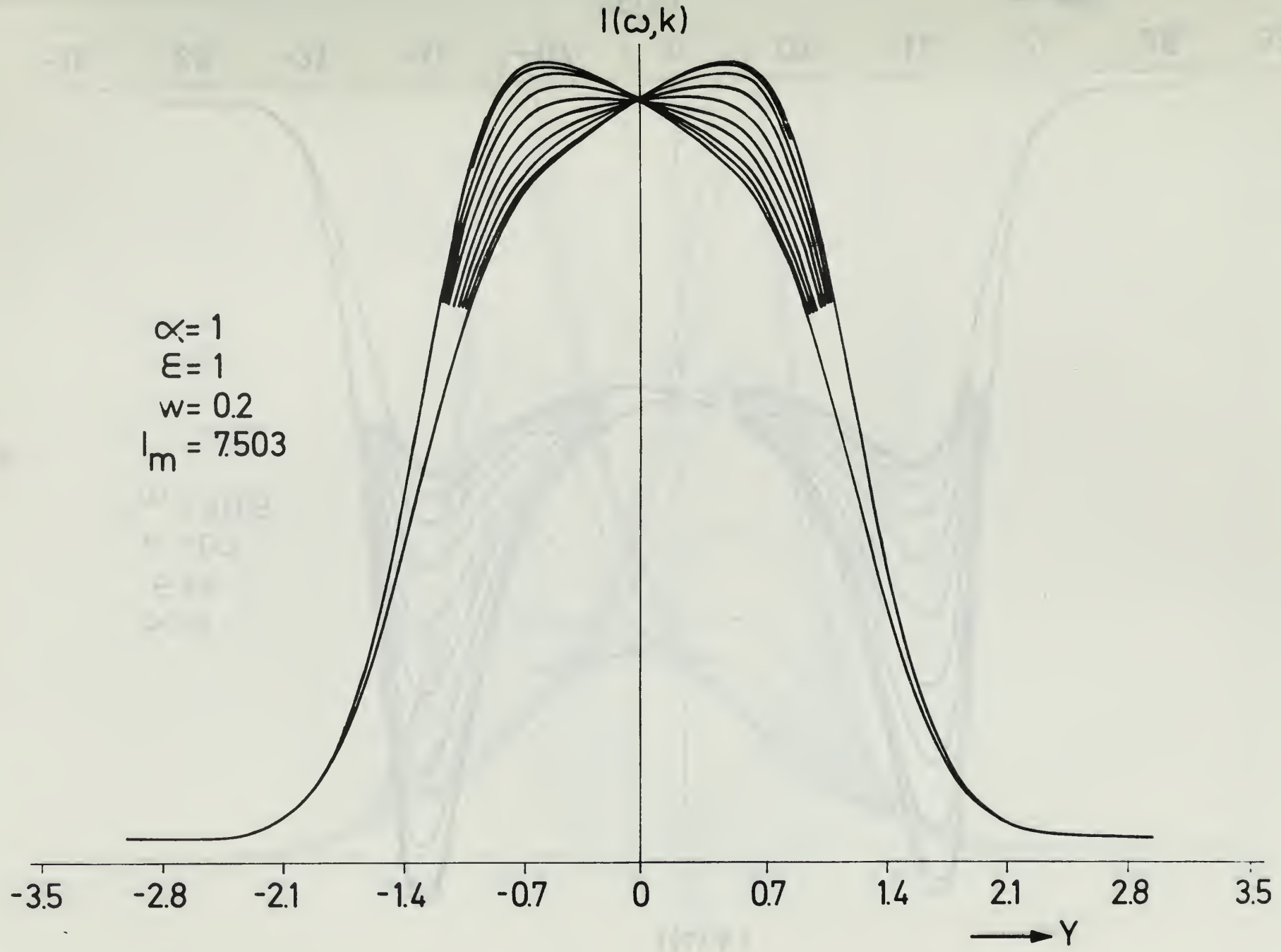
I(ω,k)
α= 1
ε= 1
w= 0.2
I_m = 7.503
-3.5
-2.8
-2.1
-1.4
-0.7
0
0.7
1.4
2.1
2.8
3.5
Y

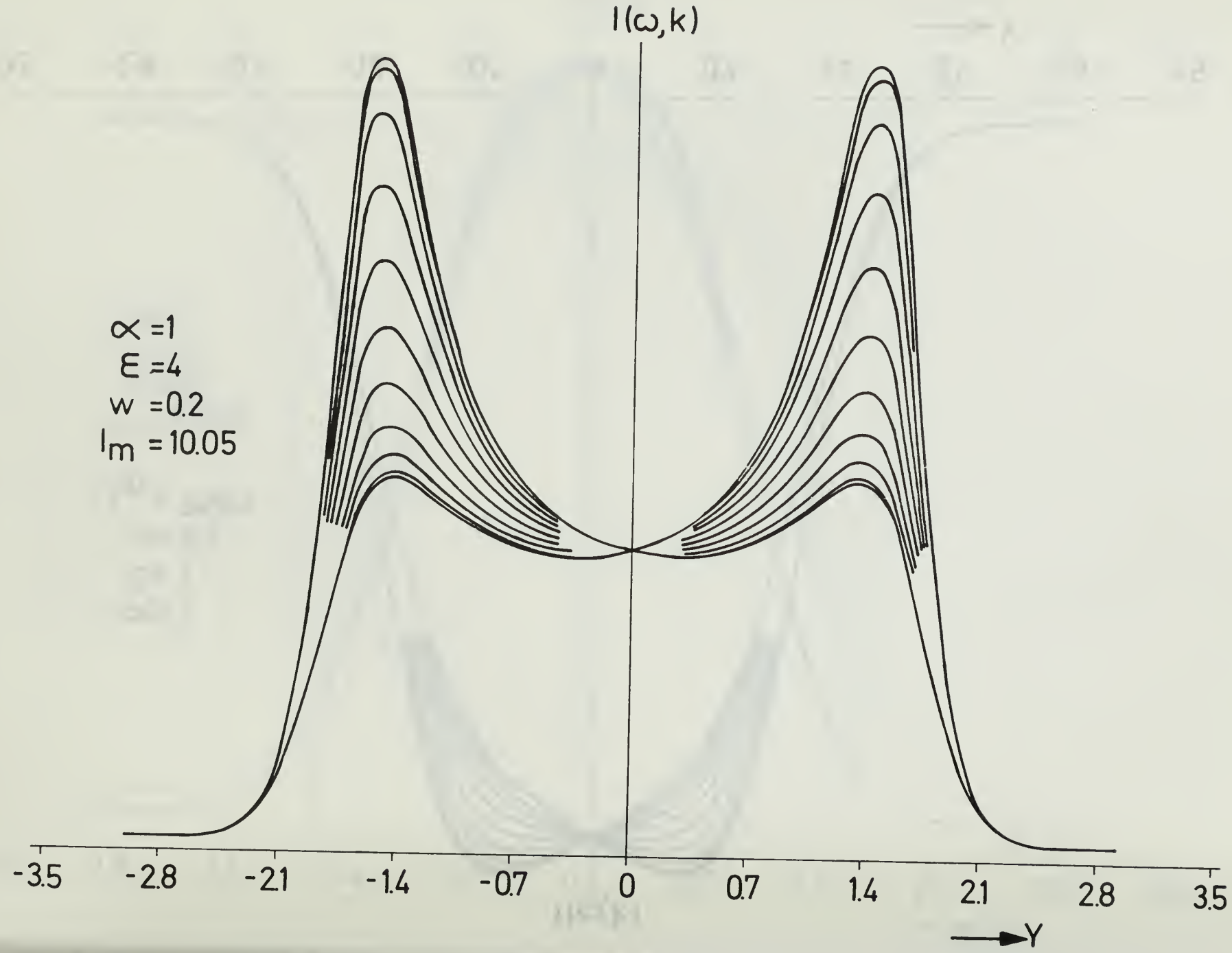
I(ω,k)
α =1
ε =4
w =0.2
Im = 10.05
-3.5
-2.8
-2.1
-1.4
-0.7
0
0.7
1.4
2.1
2.8
3.5
Y

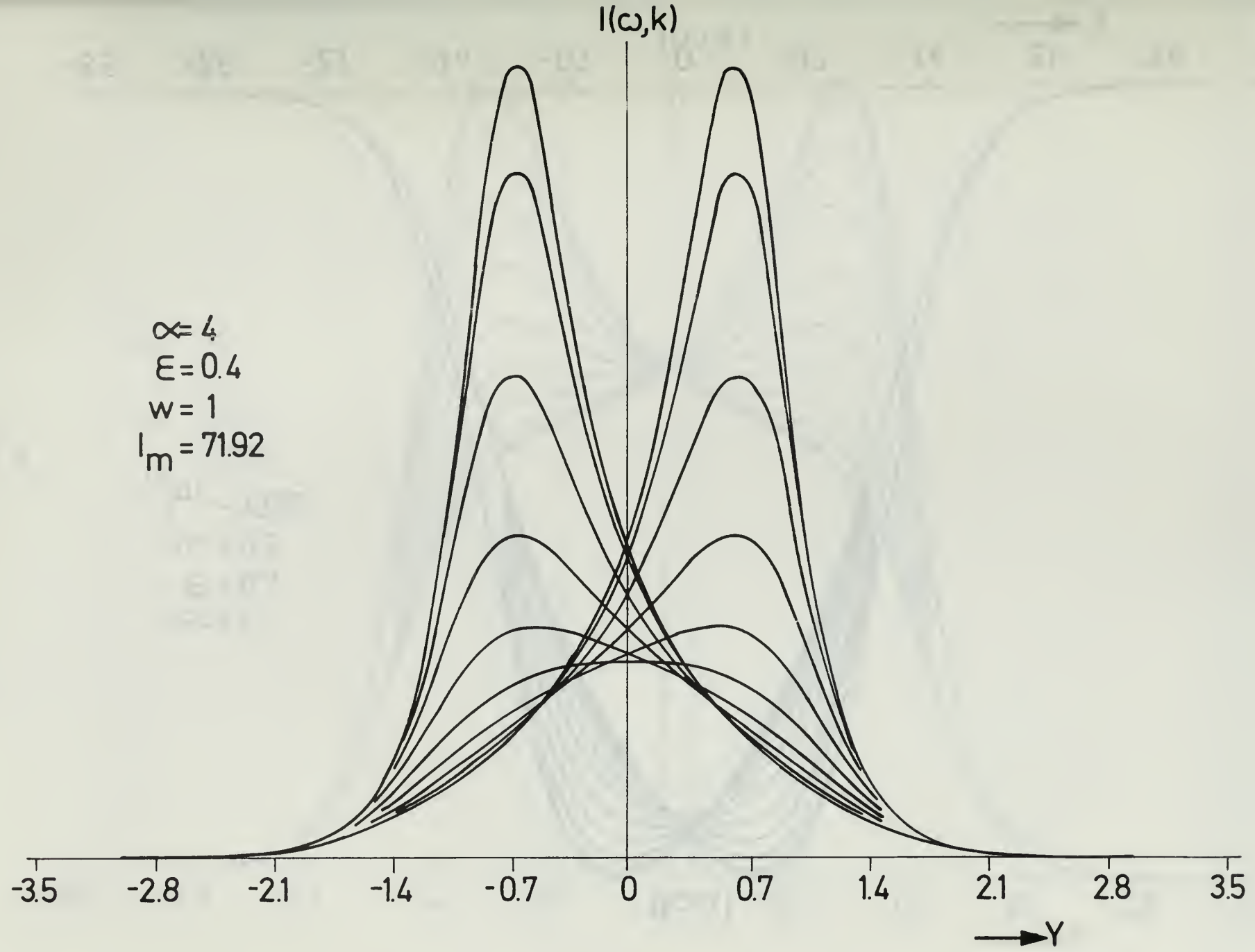
I(ω,k)
∝= 4
ε = 0.4
w = 1
I_m = 71.92
-3.5
-2.8
-2.1
-1.4
-0.7
0
0.7
1.4
2.1
2.8
3.5
Y

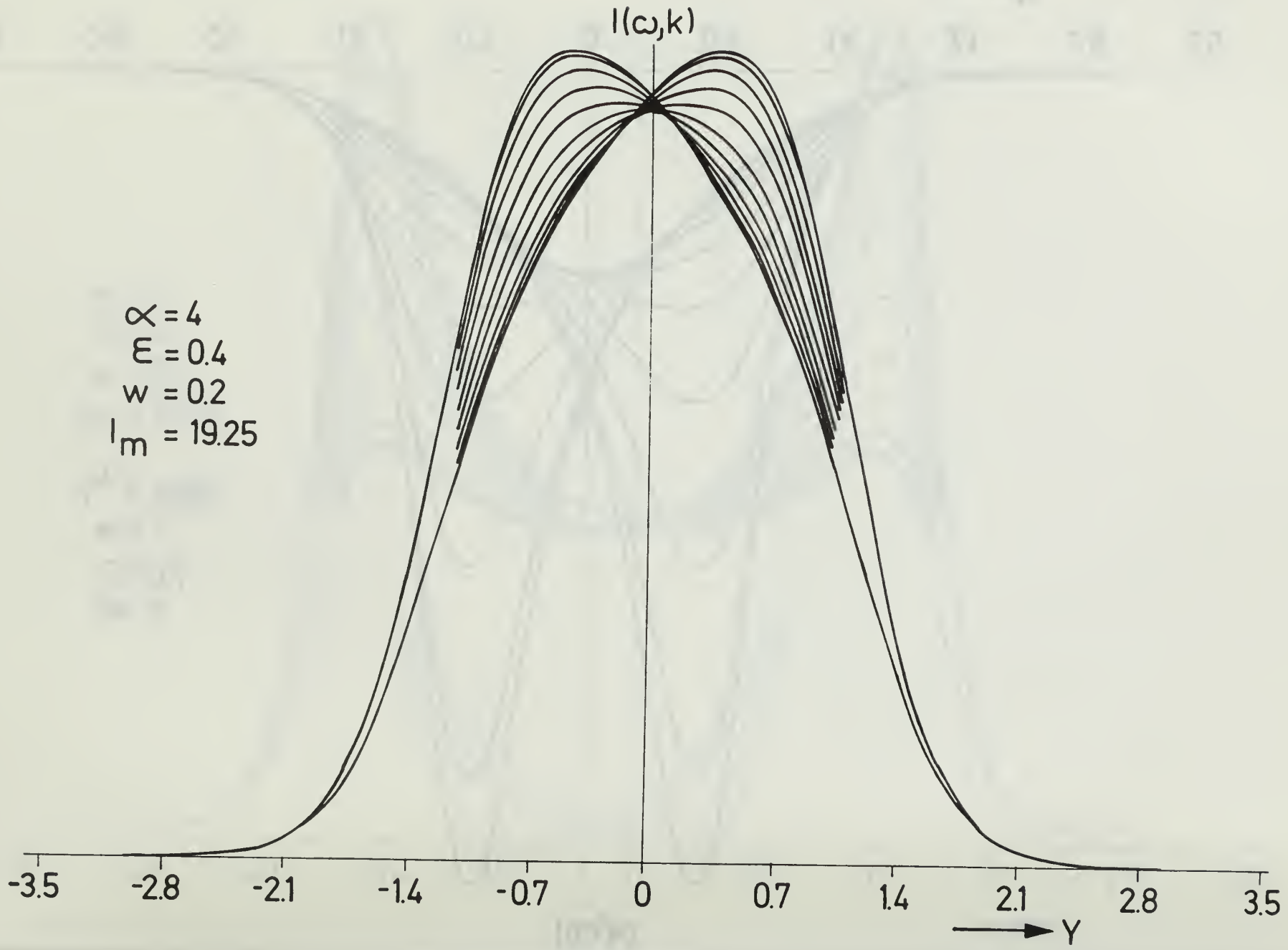
I(ω,k)
∝ = 4
ε = 0.4
w = 0.2
I_m = 19.25
-3.5
-2.8
-2.1
-1.4
-0.7
0
0.7
1.4
2.1
2.8
3.5
Y

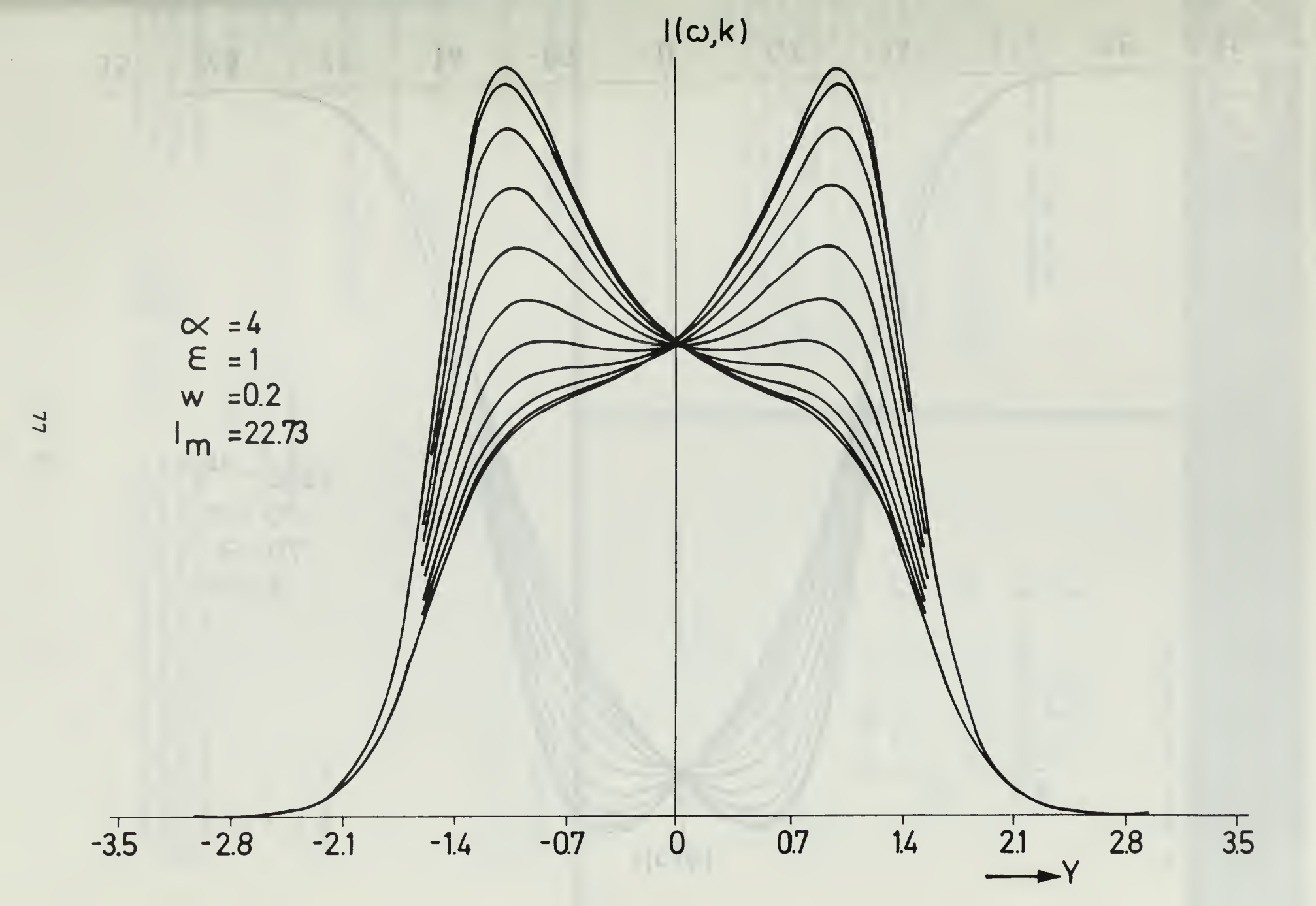
I(ω,k)
α =4
ε =1
w =0.2
I_m =22.73
-3.5
-2.8
-2.1
-1.4
-0.7
0
0.7
1.4
2.1
2.8
3.5
Y

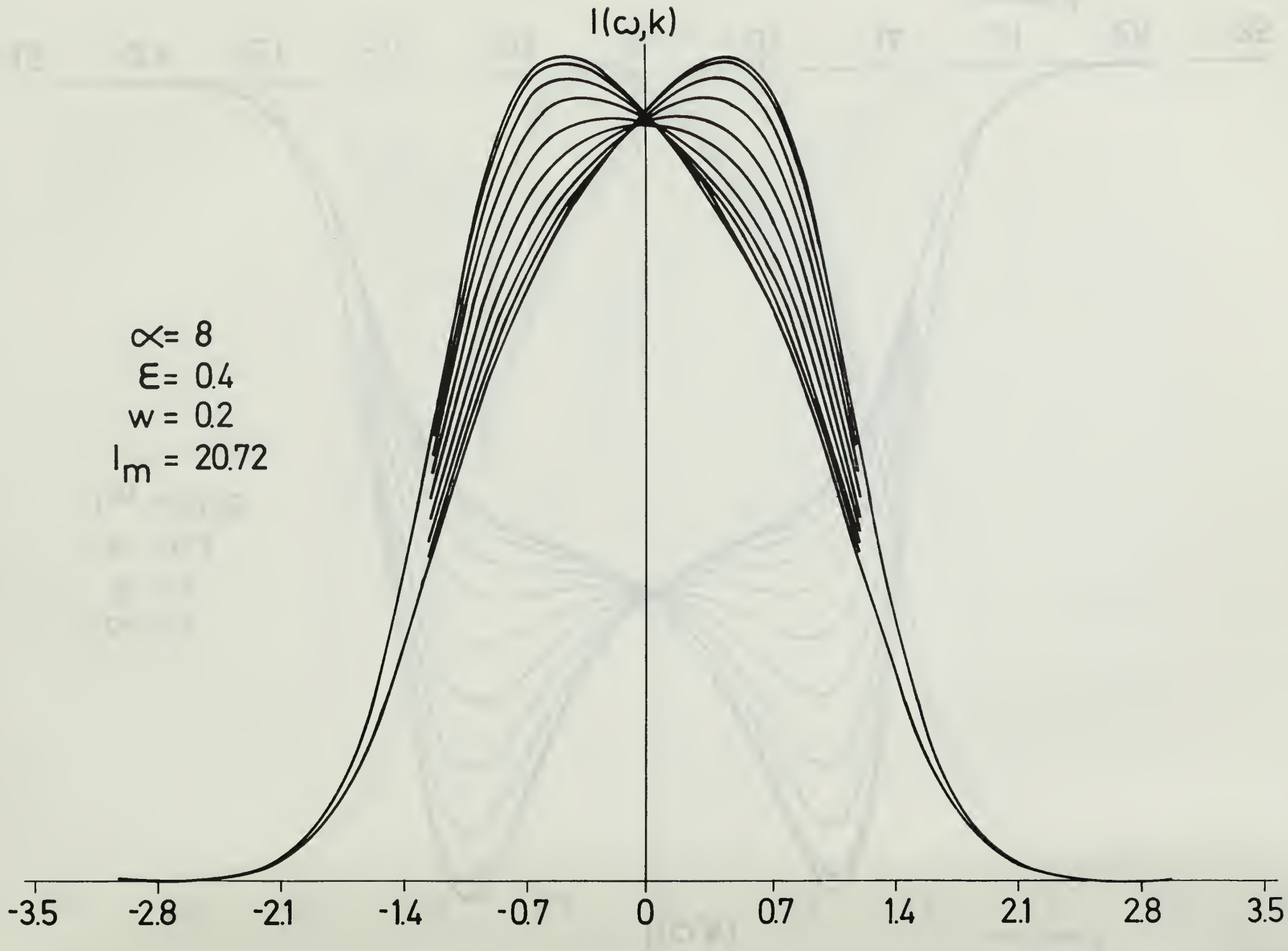
I(ω,k)
∝= 8
ε= 0.4
w = 0.2
I_m = 20.72
-3.5
-2.8
-2.1
-1.4
-0.7
0
0.7
1.4
2.1
2.8
3.5

TECHNICAL DATA 15 FEB 66

ULTRAFAST LOW NOISE SILICON PIN PHOTODIODE

The hpa 4205 is a silicon planar PIN photodiode for etection of light in the visible and near infrared regions. esponse to blue and violet light is unusually good for a ery low, dark current silicon photodiode.

Speed of response of this diode is less than 1 nanosecond. aser pulses shorter than 0.1 nanosecond may be observed. he frequency response extends from DC to 1 gc.

The low dark current of less than 150 picoamperes en- les detection of very low light levels. The quantum detec- on efficiency is constant over six decades of light intensity, roving excellent dynamic range.

An extremely fast photon coupled pair can be obtained using the hpa 4205 in conjunction with the hpa 4107 nfrared light source in an identical package), for con- enient use in card and tape readers, encoders, and similar pplications.

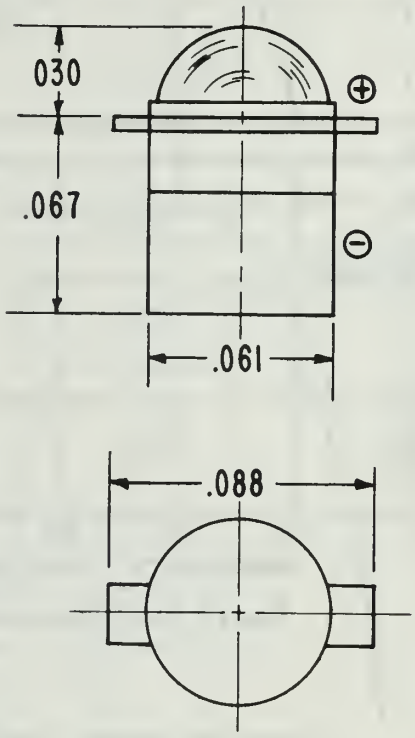

OPTICAL CHARACTERISTICS

		Test Conditions
Response at 7700 Å	0.75 electrons/photon 0.25 μA/mW/cm^2 0.125 μA/μW	V = — 20 v R_L = < 1 MΩ
Sensitive Area	0.5 x 10^{-3} cm^2 0.010″ diameter	
Speed of Response	Less than 1 nanosecond	

ELECTRICAL CHARACTERISTICS (25°C)

		Test Conditions
Dark Current	150 picoamps maximum	V_R = — 10 volts
Forward Current	50 mA minimum	V_F = 1 volt
Capacitance	0.7 pf typical	V_R = — 10 V

MAXIMUM RATINGS

Steady Reverse Voltage ..... 50 volts
Peak Inverse Voltage ..... 200 volts (see Note)
Power Dissipation ..... 50 mW T = 25°C

Note: Exceeding the PIV will cause permanent damage to the diode. Forward current is harmless to the diode, within the power dissipation limit. For optimum performance, the diode should be reverse biased at between 5 and 20 volts.

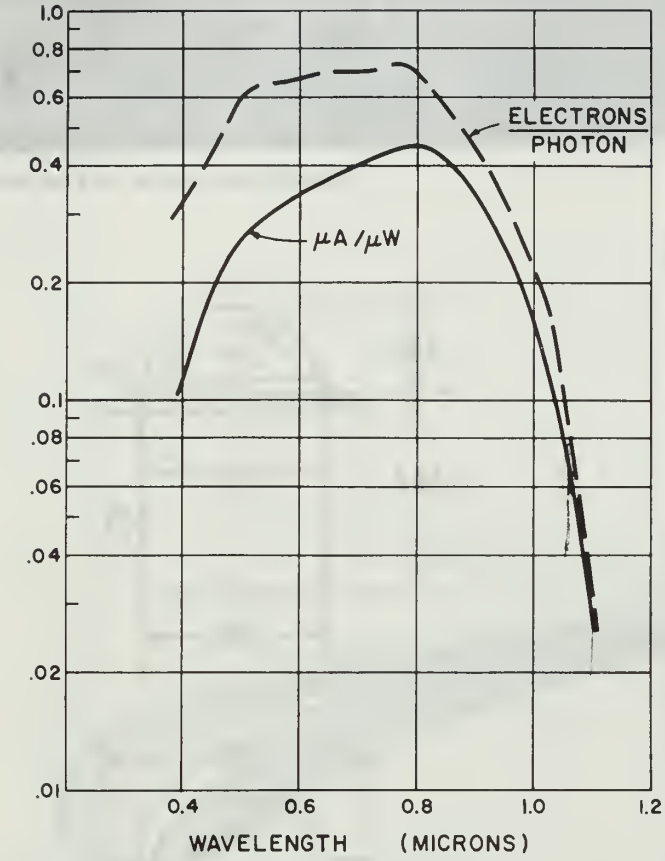

Figure 1. Spectral Response

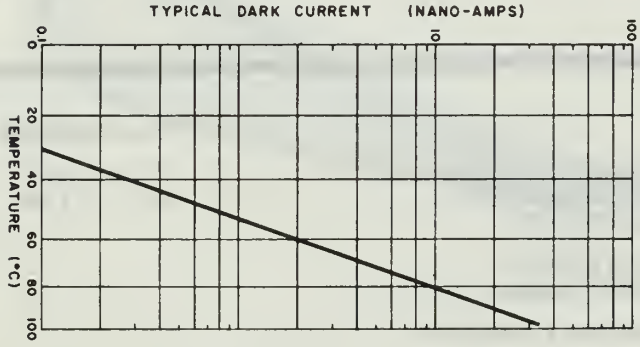

Figure 2. Dependence of Dark Current on Temperature

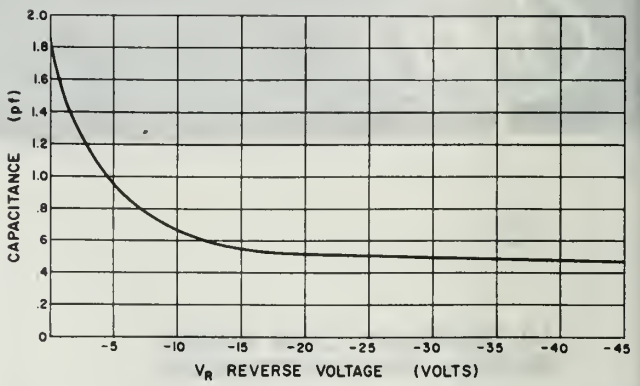

Figure 3. Typical Capacitance Variation with Reverse Bias (f = 1 mc)

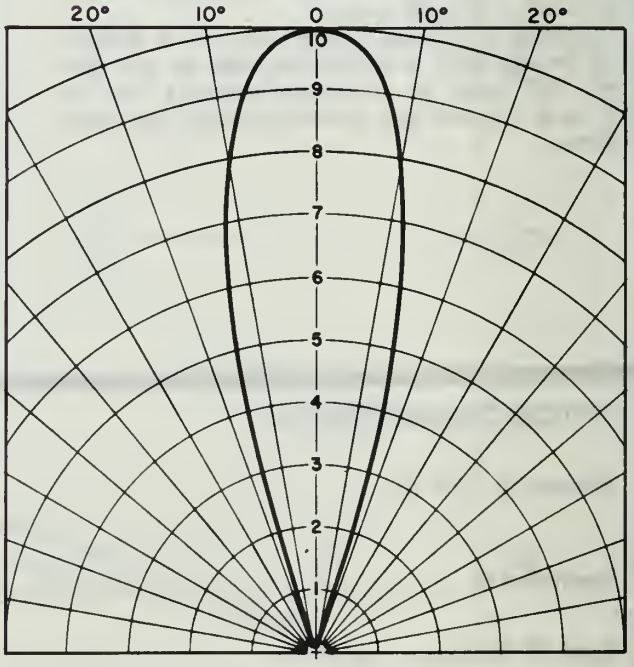

Figure 4. Relative Directional Sensitivity

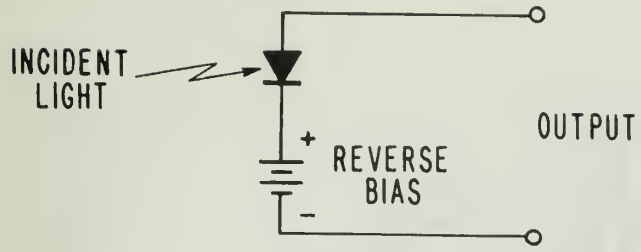

Figure 5. Schematic Diagram.

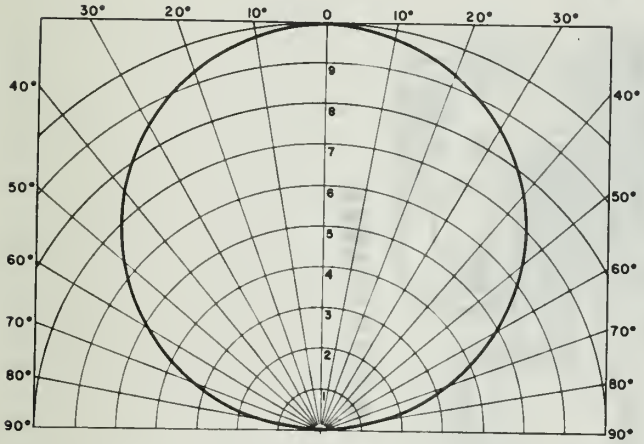

Figure 6. Relative Directional Sensitivity of the PIN Photodiodes.

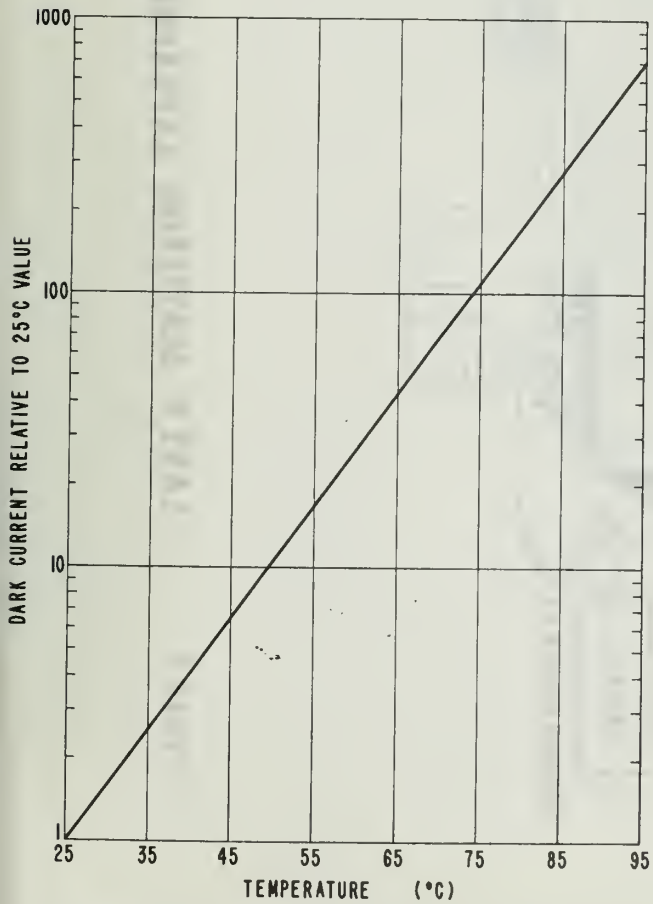

Figure 7. Dark Current at — 10 V Bias vs. Temperature.

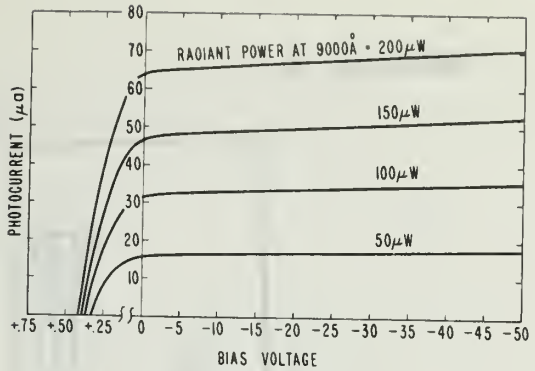

Figure 8. Typical Output Characteristics.

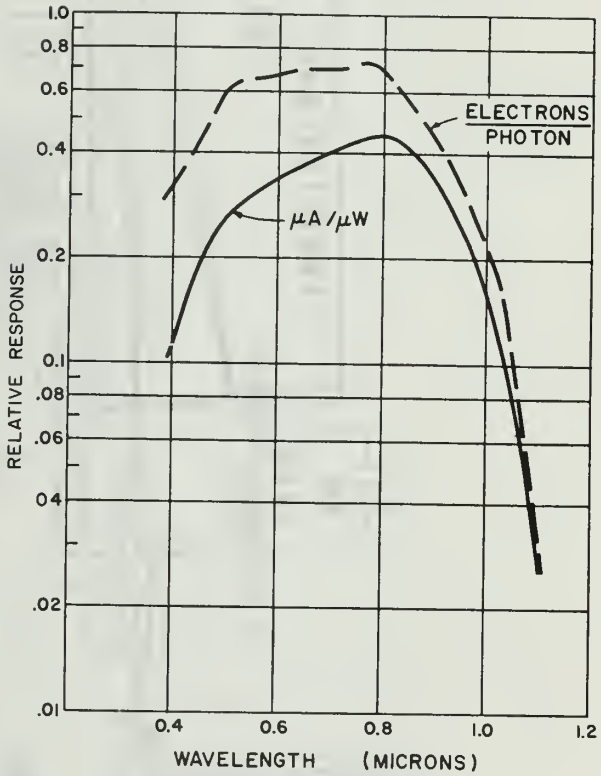

Figure 9. Spectral Response.

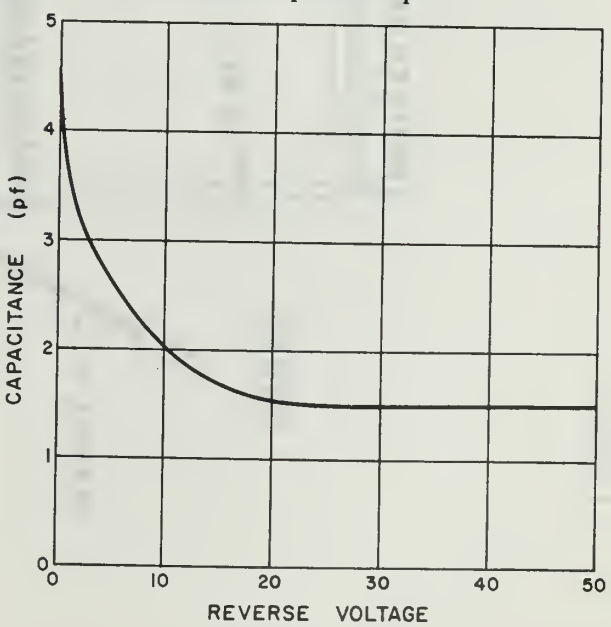

Figure 10. Typical Capacitance Variation with Applied Voltage.

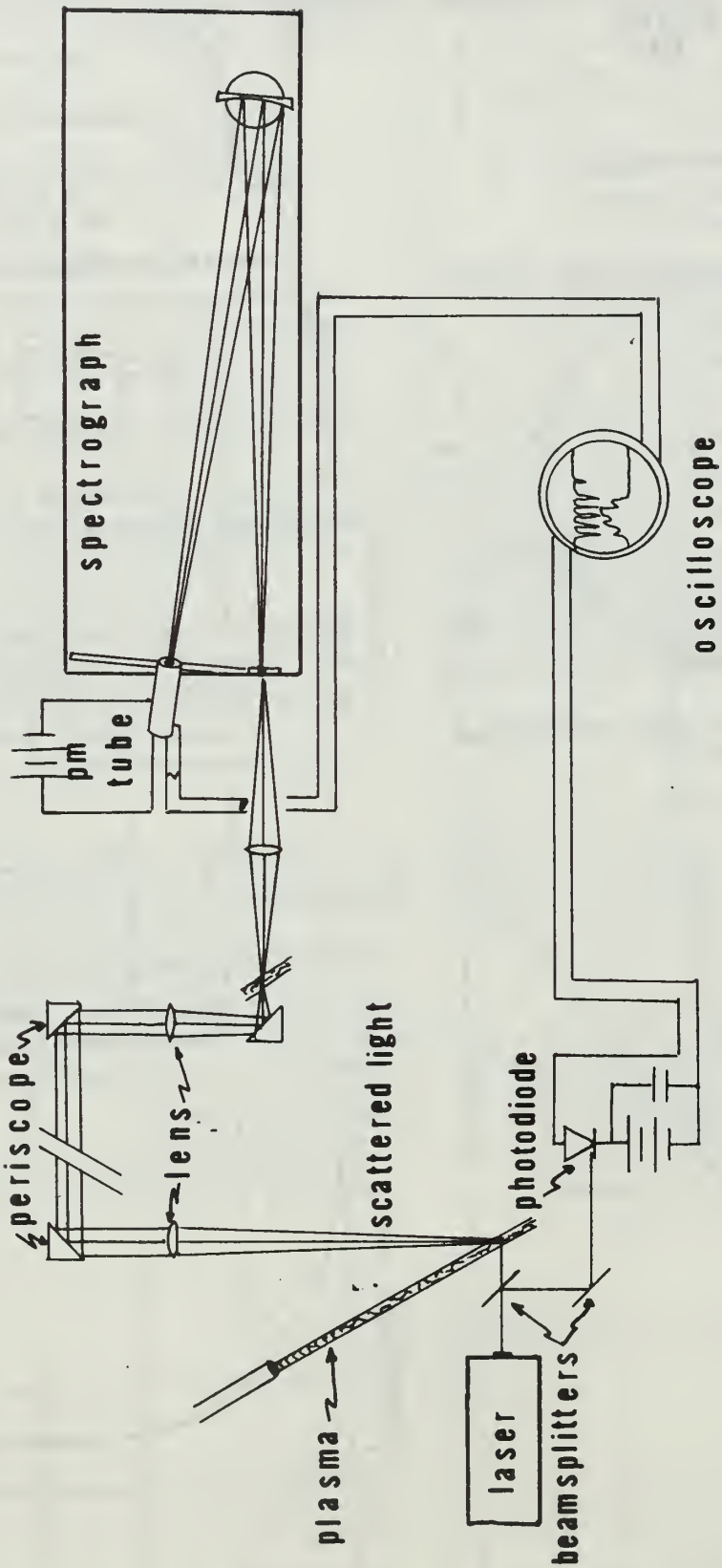

figure I LASER SCATTERING EXPERIMENT

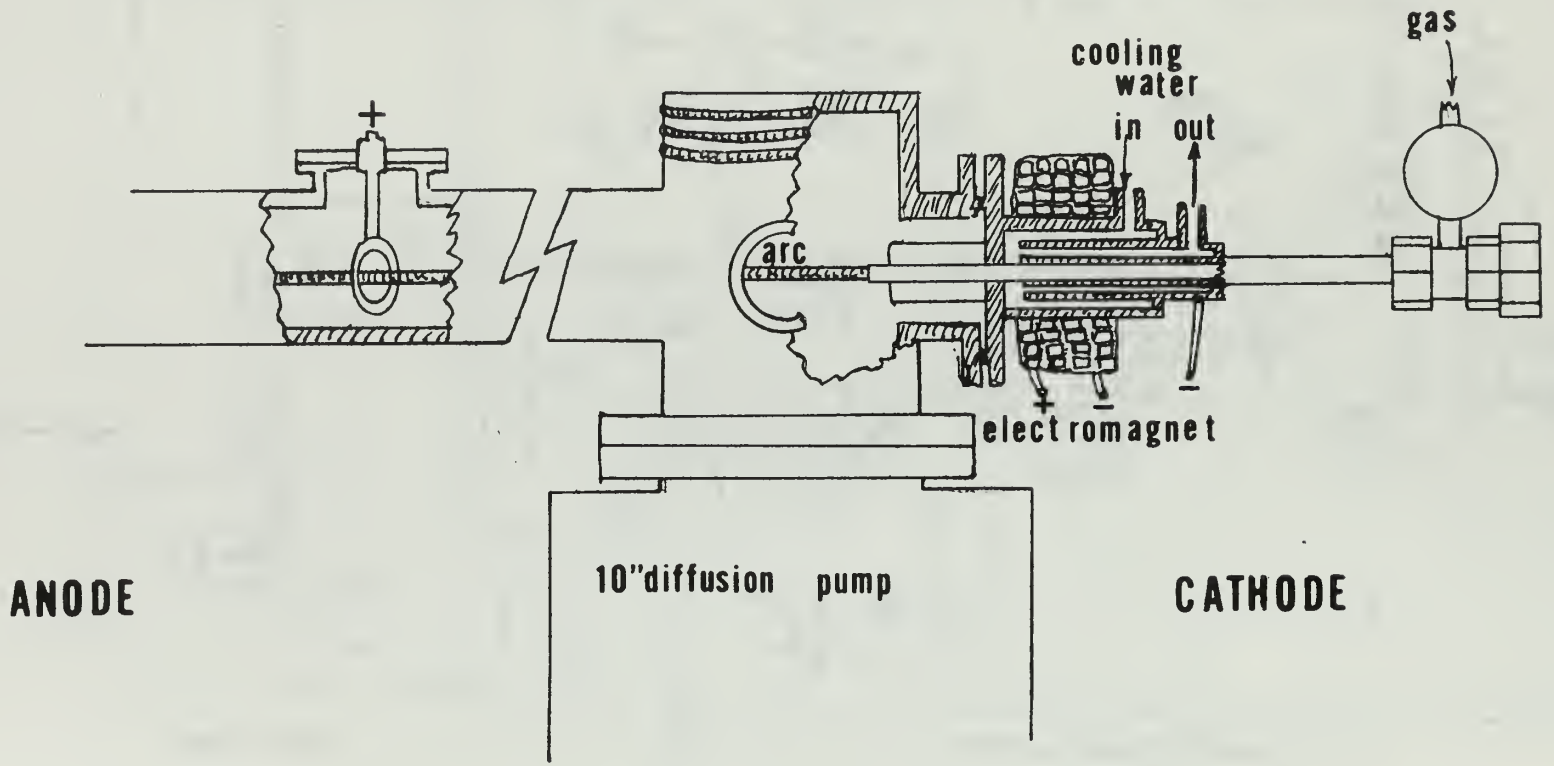
gas
cooling
water
in
out
arc
+
−
electromagnet
ANODE
10"diffusion pump
CATHODE

figure 2

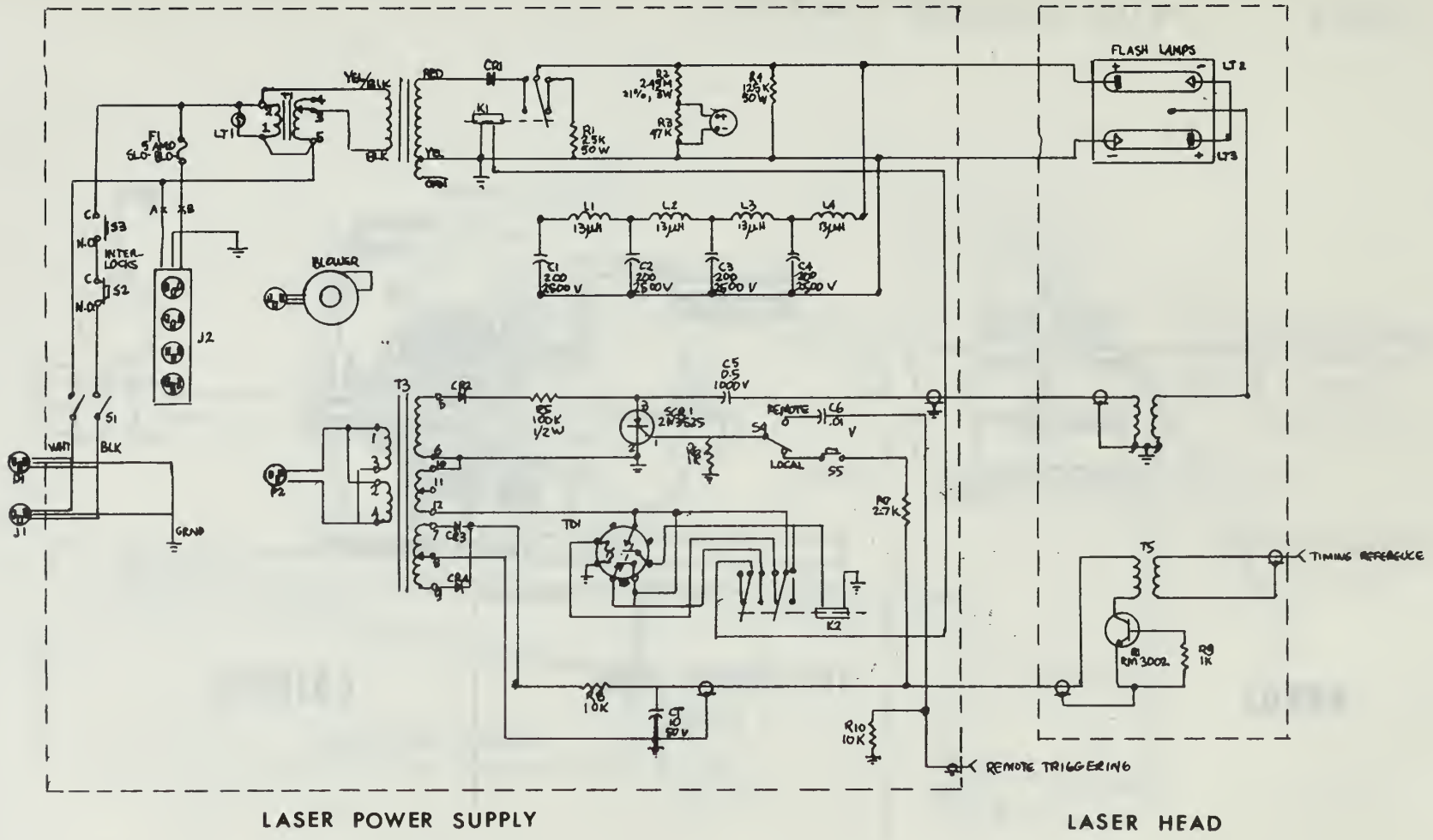
FLASH LAMPS
LT2
LT3
LT1
F1
5 AMP
SLO-BLO
YEL/BLK
RED
BLK
YEL
CR1
K1
R1
2.5K
50W
R2
249K
1%, 1W
R3
47K
R4
125K
50W
L1
13μH
L2
13μH
L3
13μH
L4
13μH
C1
200
2500 V
C2
200
2500 V
C3
200
2500 V
C4
200
2500 V
S3
INTER-
LOCKS
S2
N.O.
J2
BLOWER
T3
CR2
CR3
CR4
C5
0.5
1000 V
R5
100K
1/2W
SCR1
2N3525
REMOTE
C6
.01
V
S4
LOCAL
S5
R8
1K
R7
2.7K
TDI
K2
T5
TIMING REFERENCE
RM3002
R9
1K
R6
10K
C7
10
50 V
R10
10K
REMOTE TRIGGERING
WHT
BLK
GRND
J1
S1
LASER POWER SUPPLY
LASER HEAD

fig.3

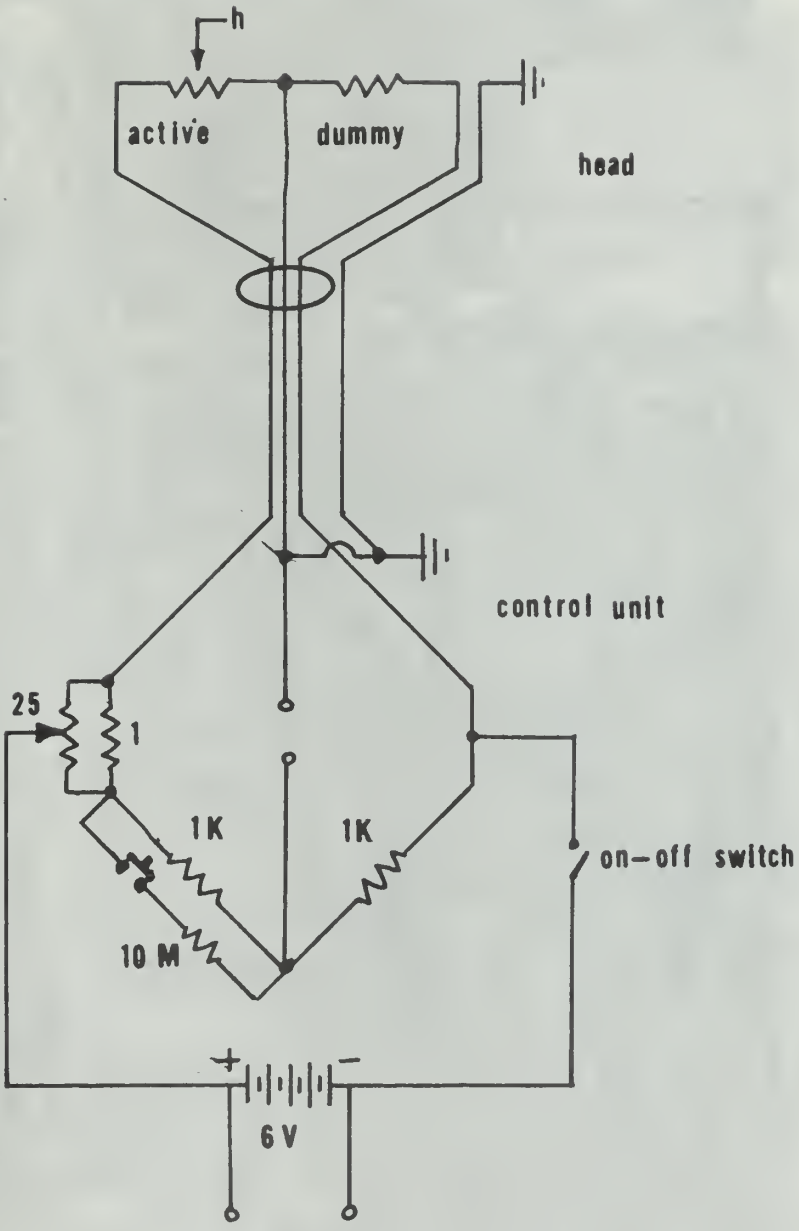

CIRCUIT SCHEMATIC OF RN-1 RADIOMETER

fig.4

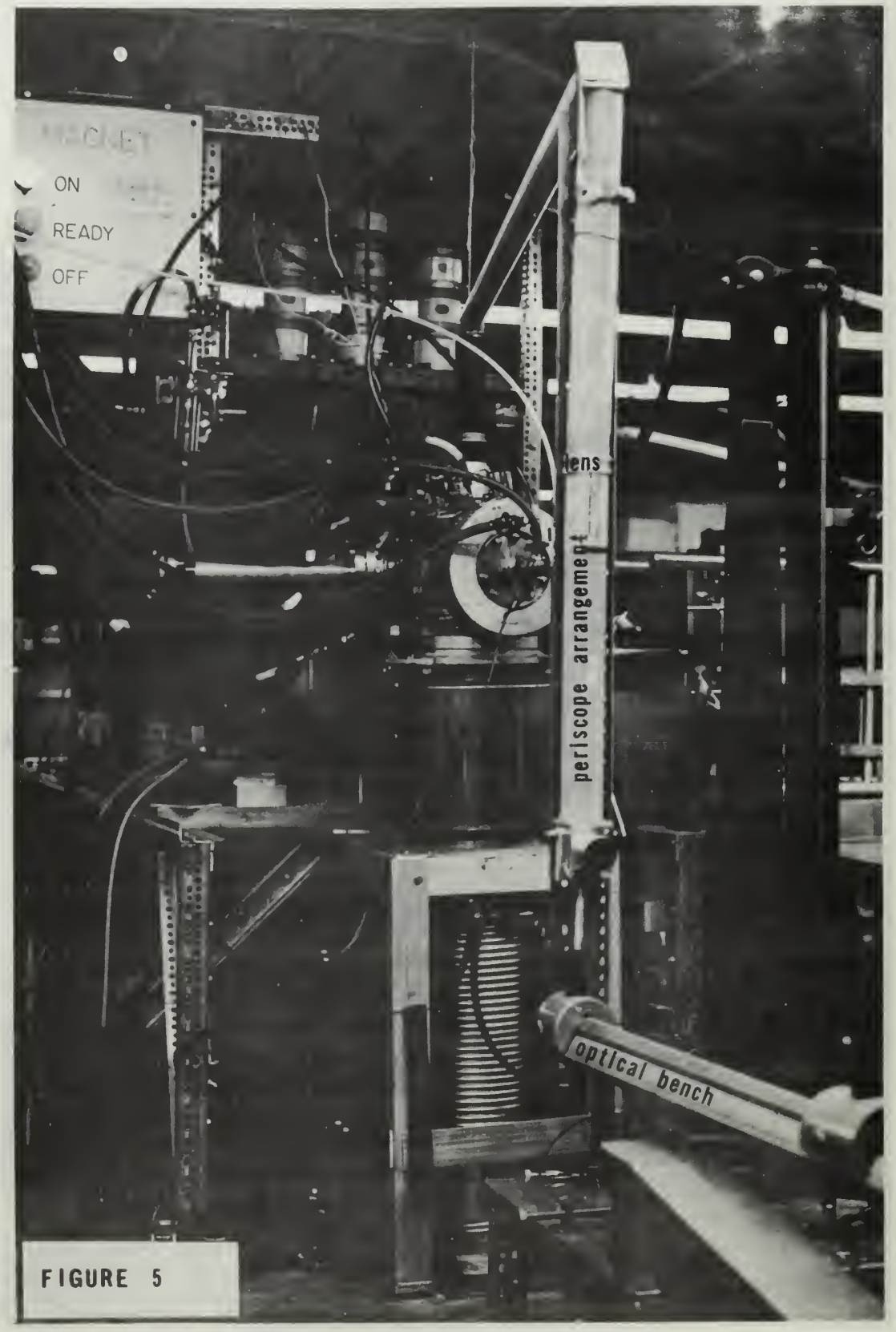

FIGURE 5

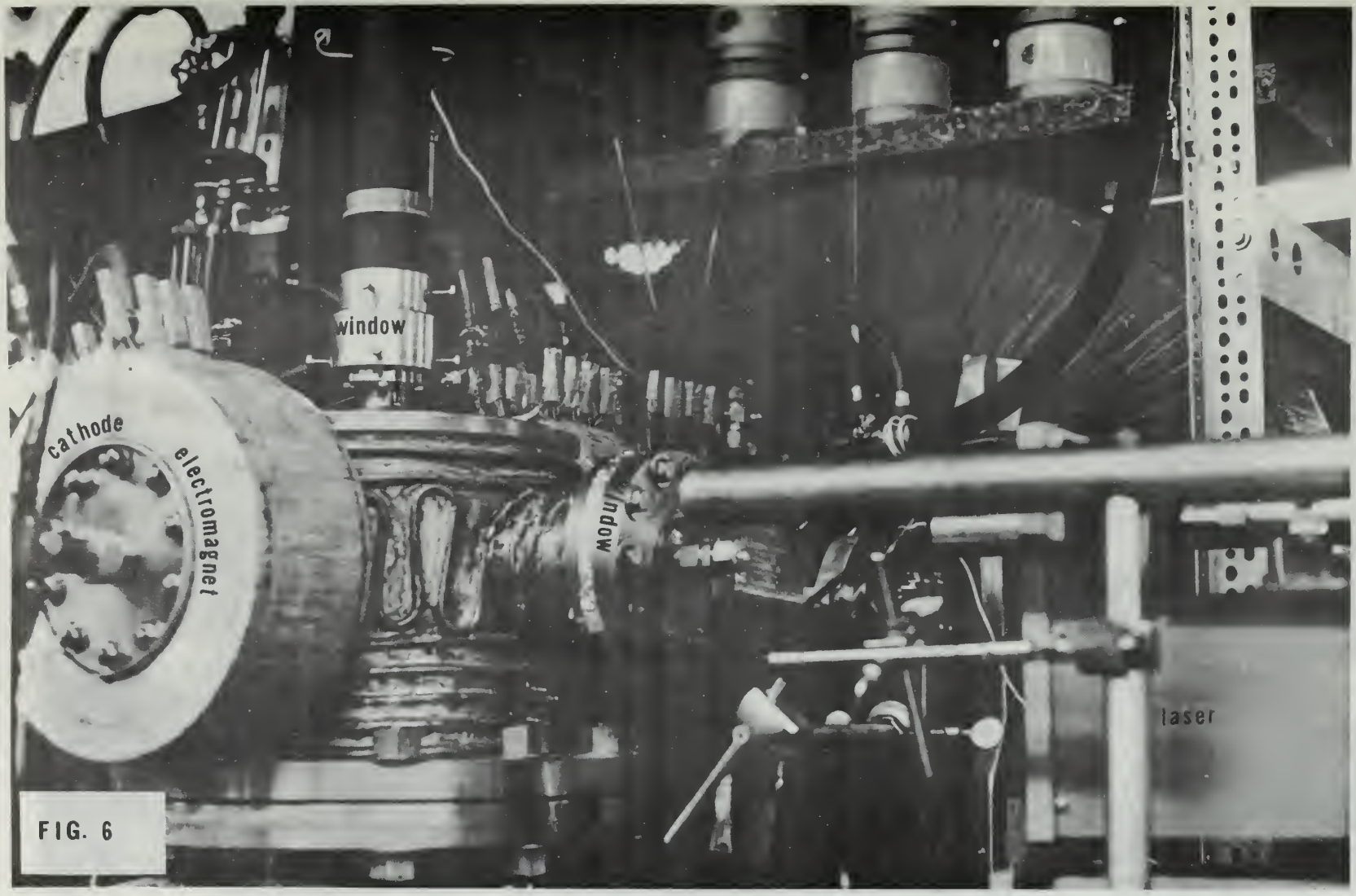

FIG. 6

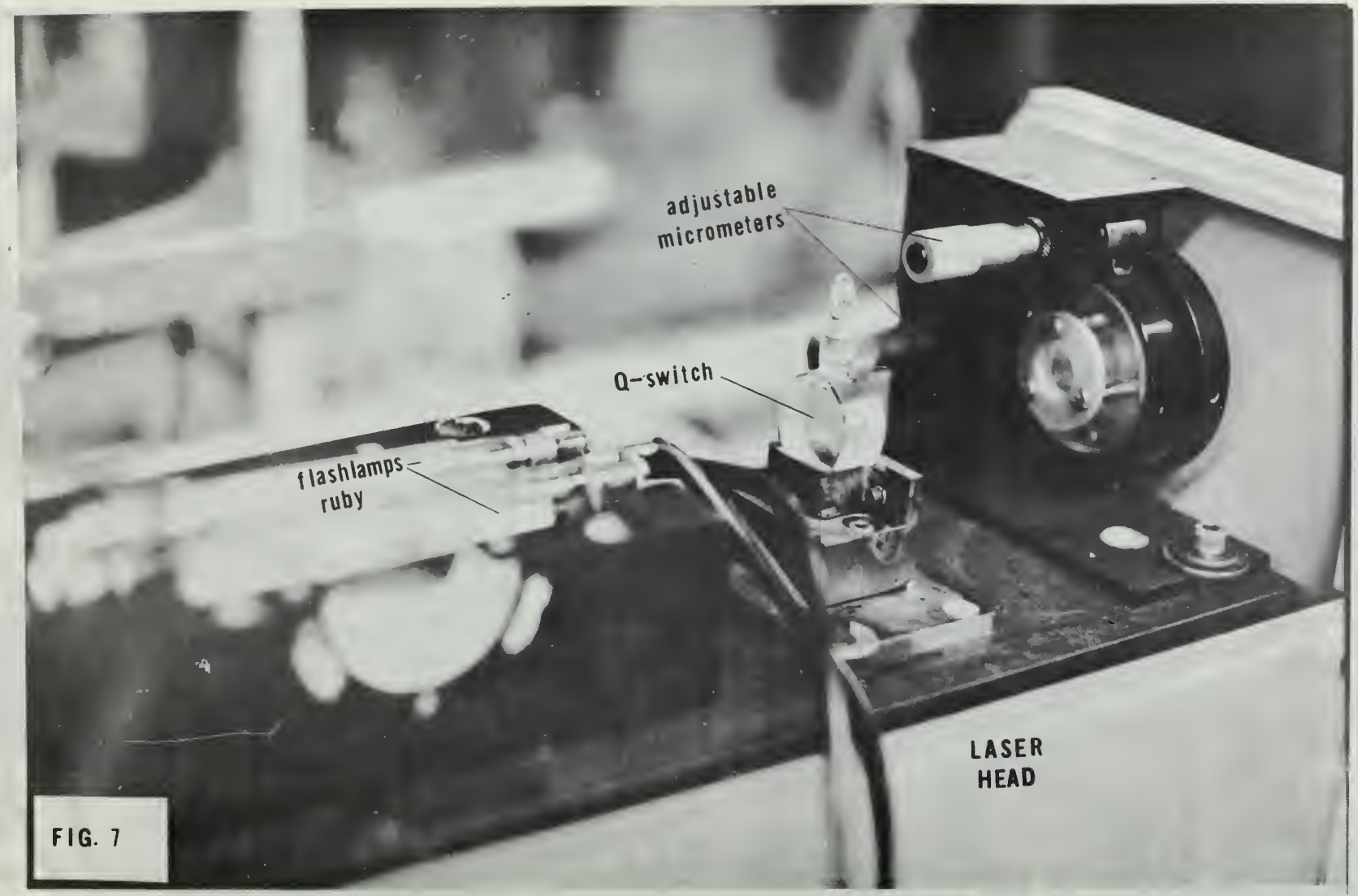
adjustable
micrometers
Q-switch
flashlamps
ruby
LASER
HEAD

FIG. 7

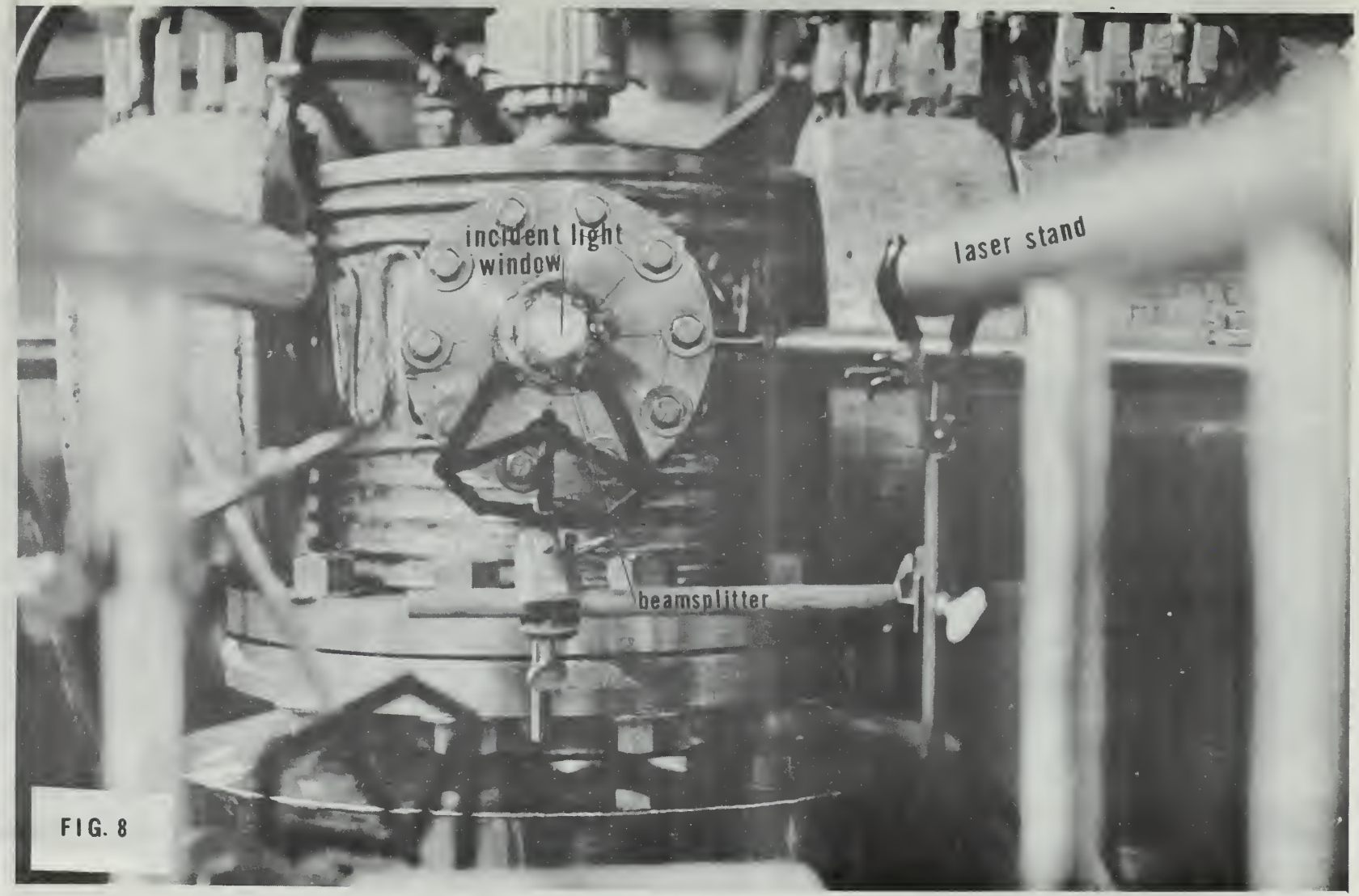

FIG. 8

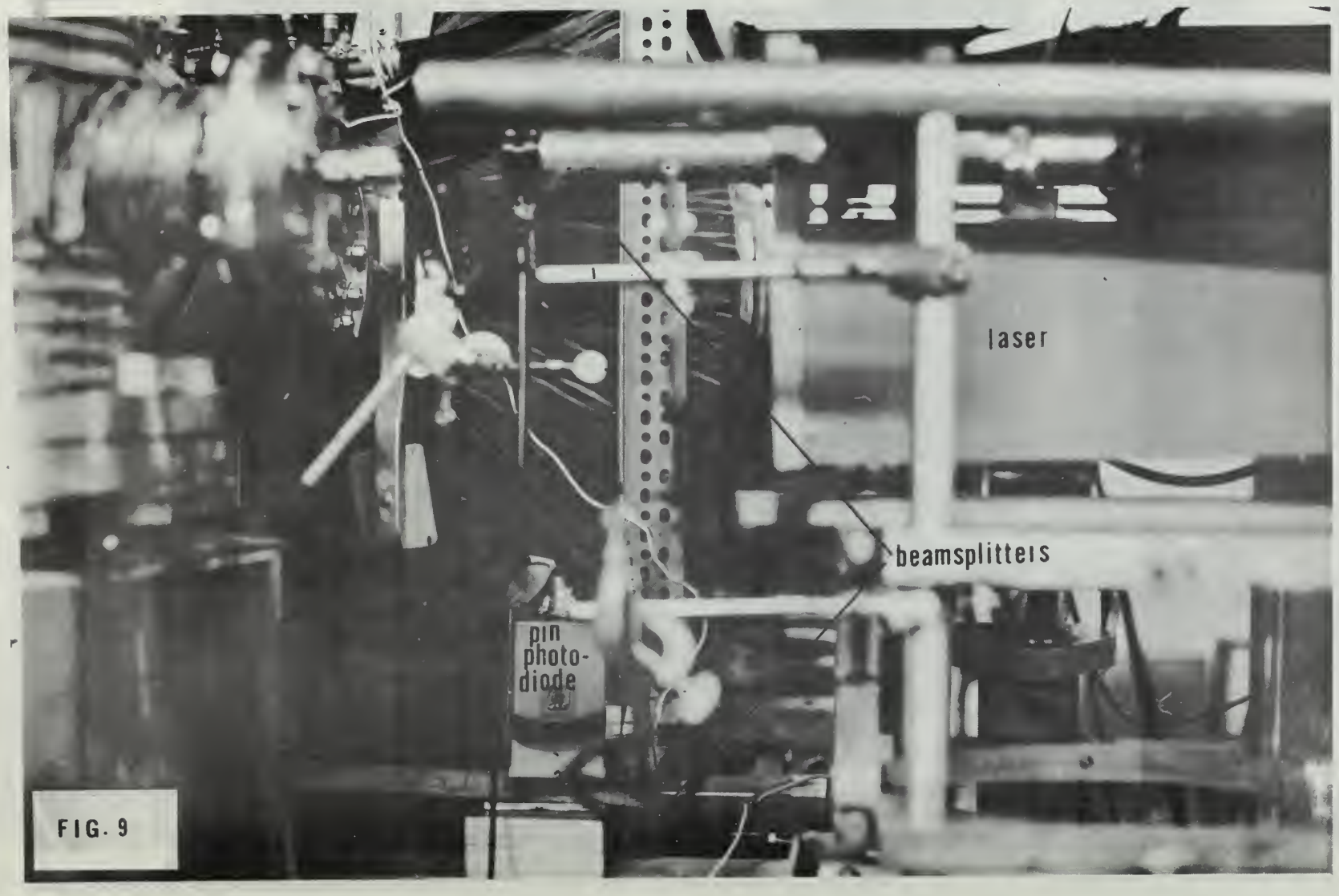

FIG. 9

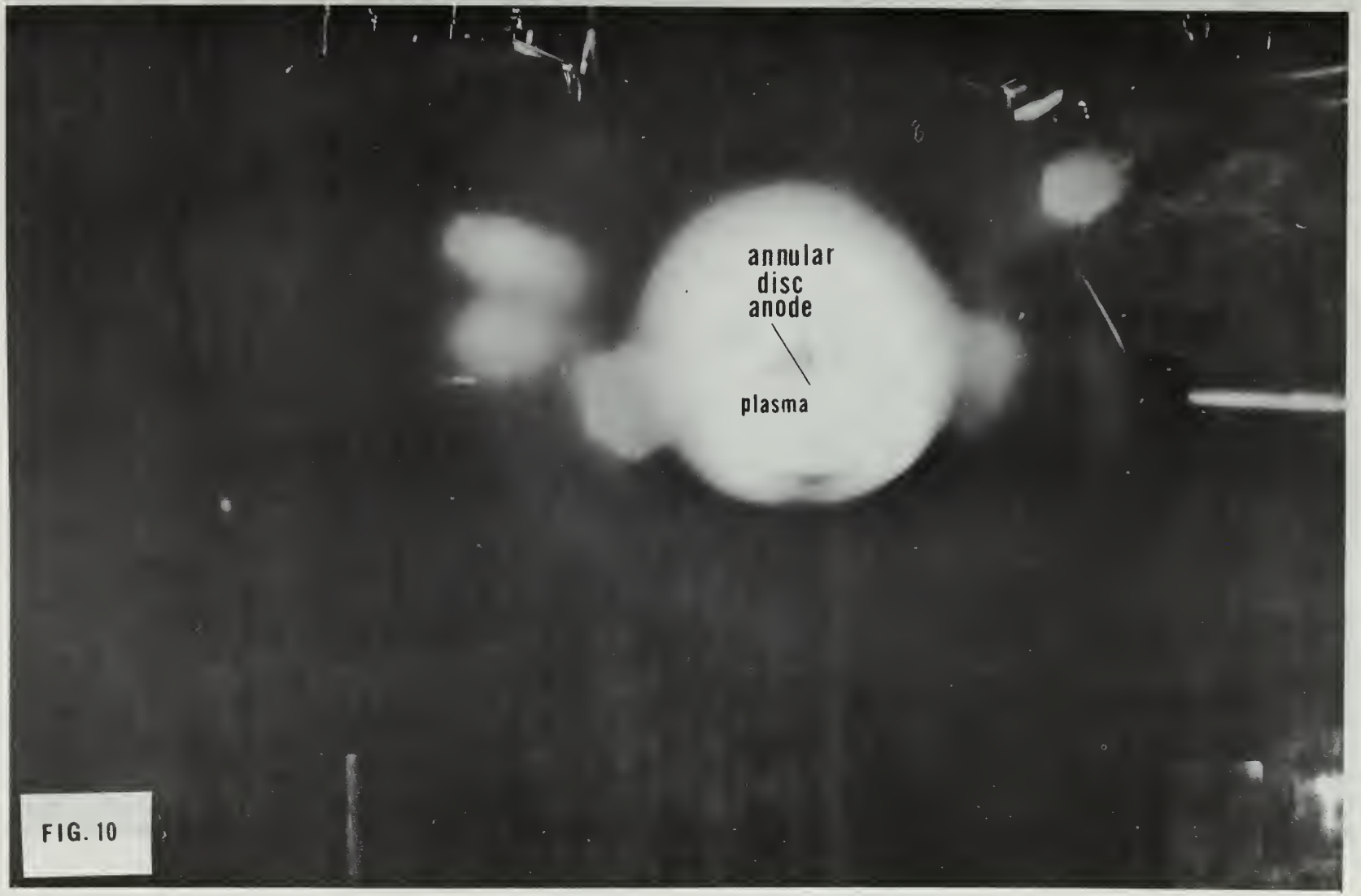

FIG. 10

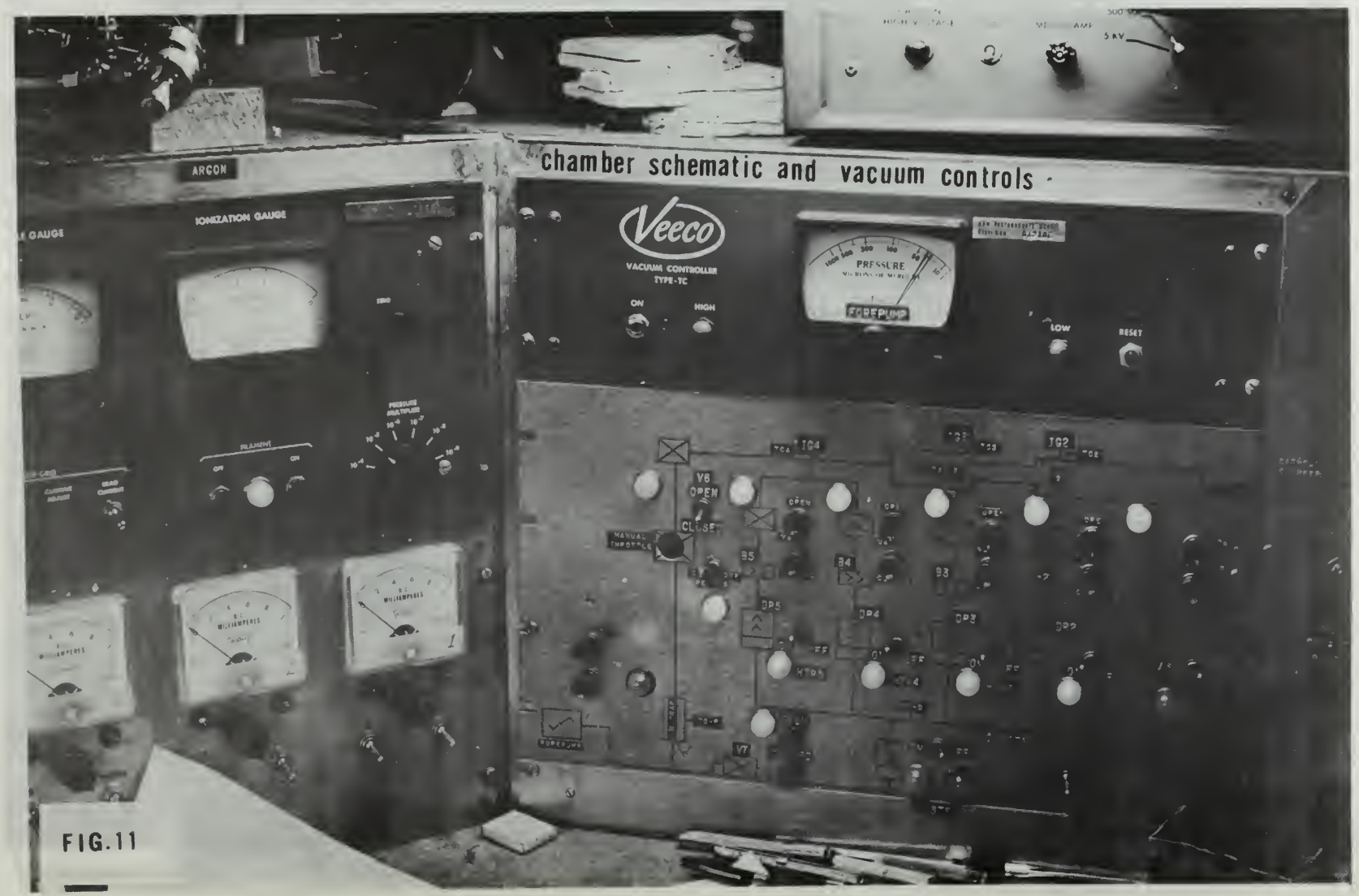
chamber schematic and vacuum controls -
ARCON
IONIZATION GAUGE
Veeco
VACUUM CONTROLLER
TYPE-TC
ON
HIGH
PRESSURE
FOREPUMP
LOW
RESET
V6
OPEN
CLOSE
MANUAL
THROTTLE
IG4
IG2
V5
V4
V3
V2
V1
DP5
DP4
DP3
DP2
FOREPUMP

FIG.11

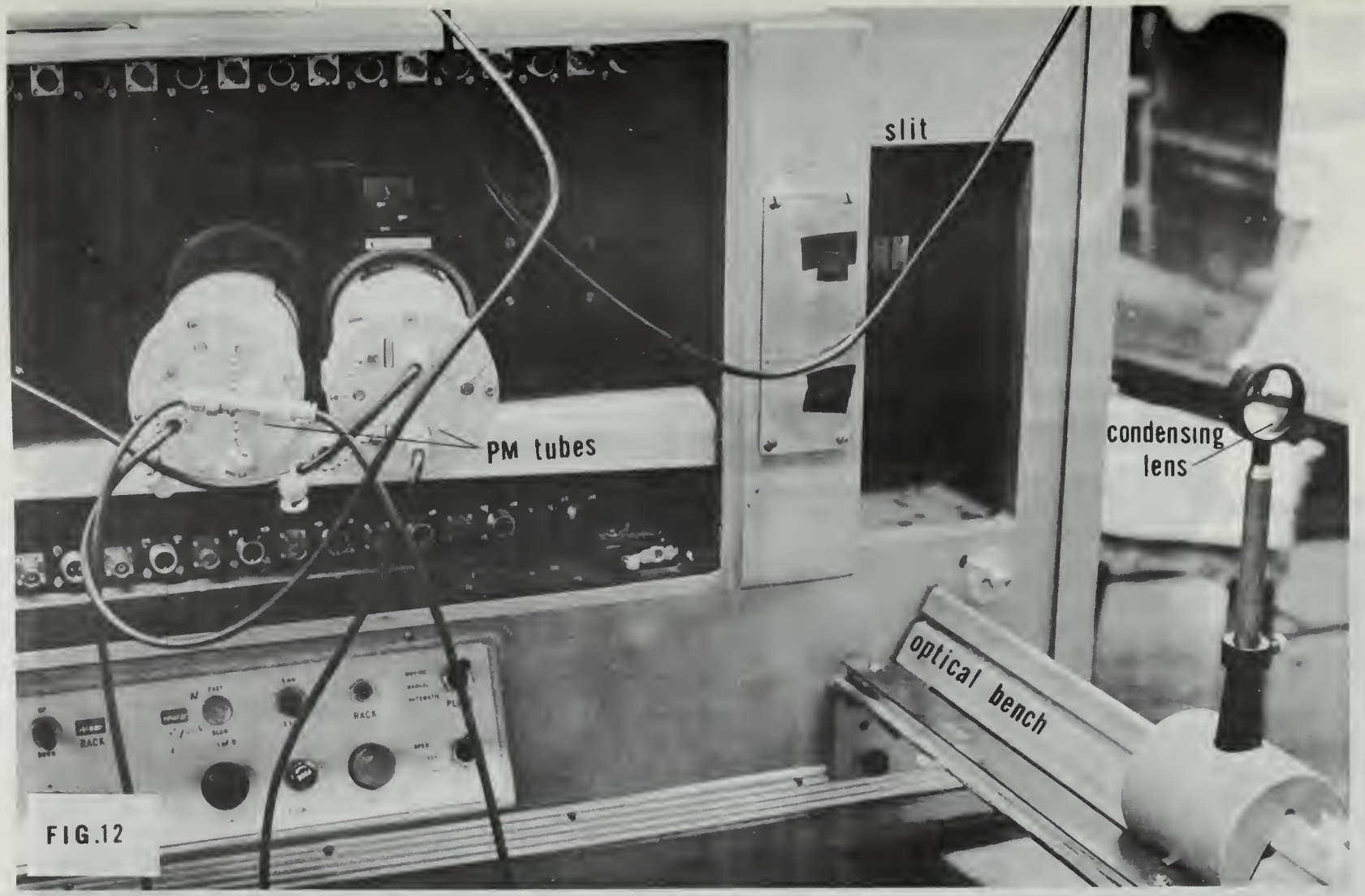

FIG.12

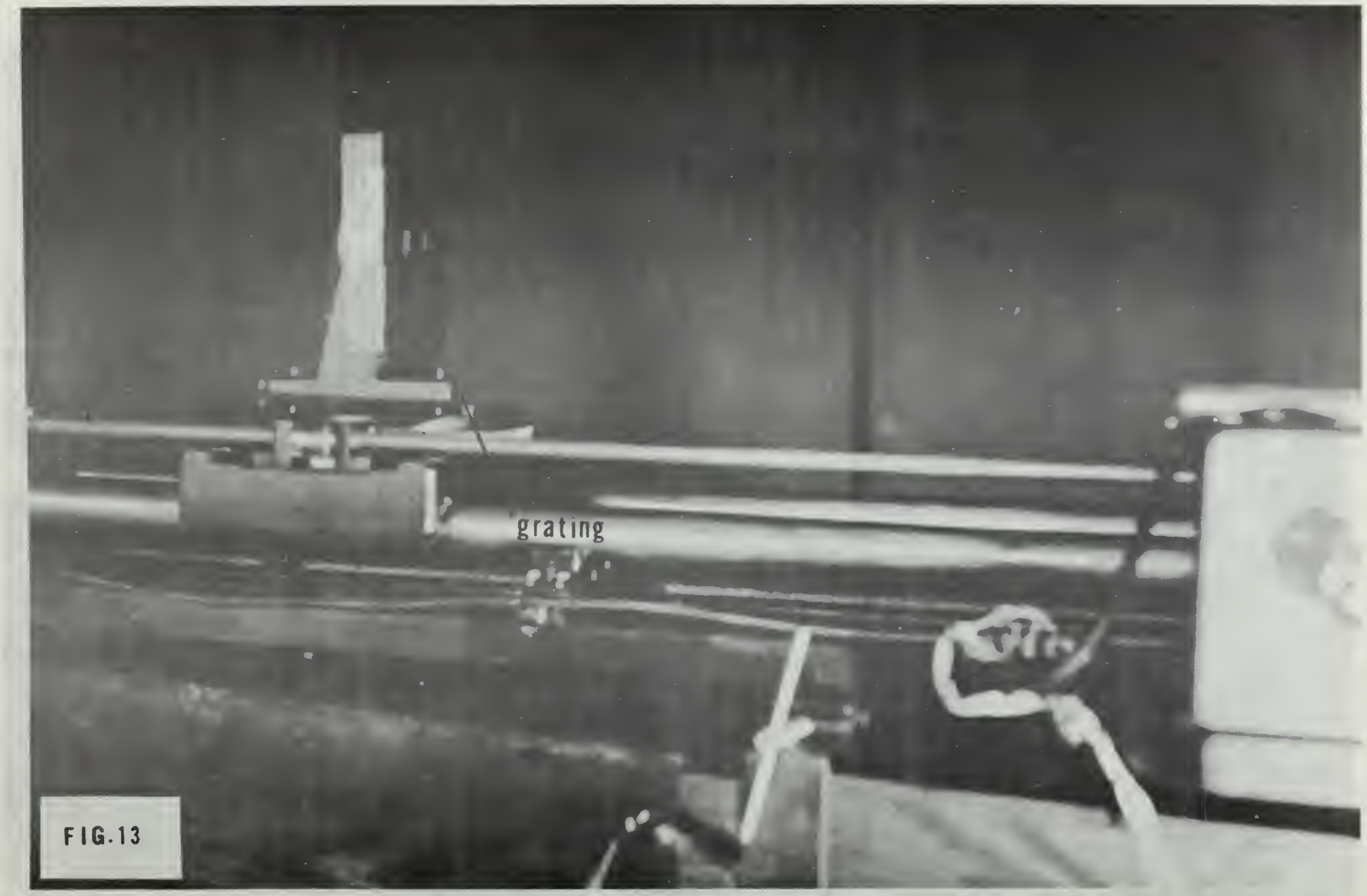

FIG. 13

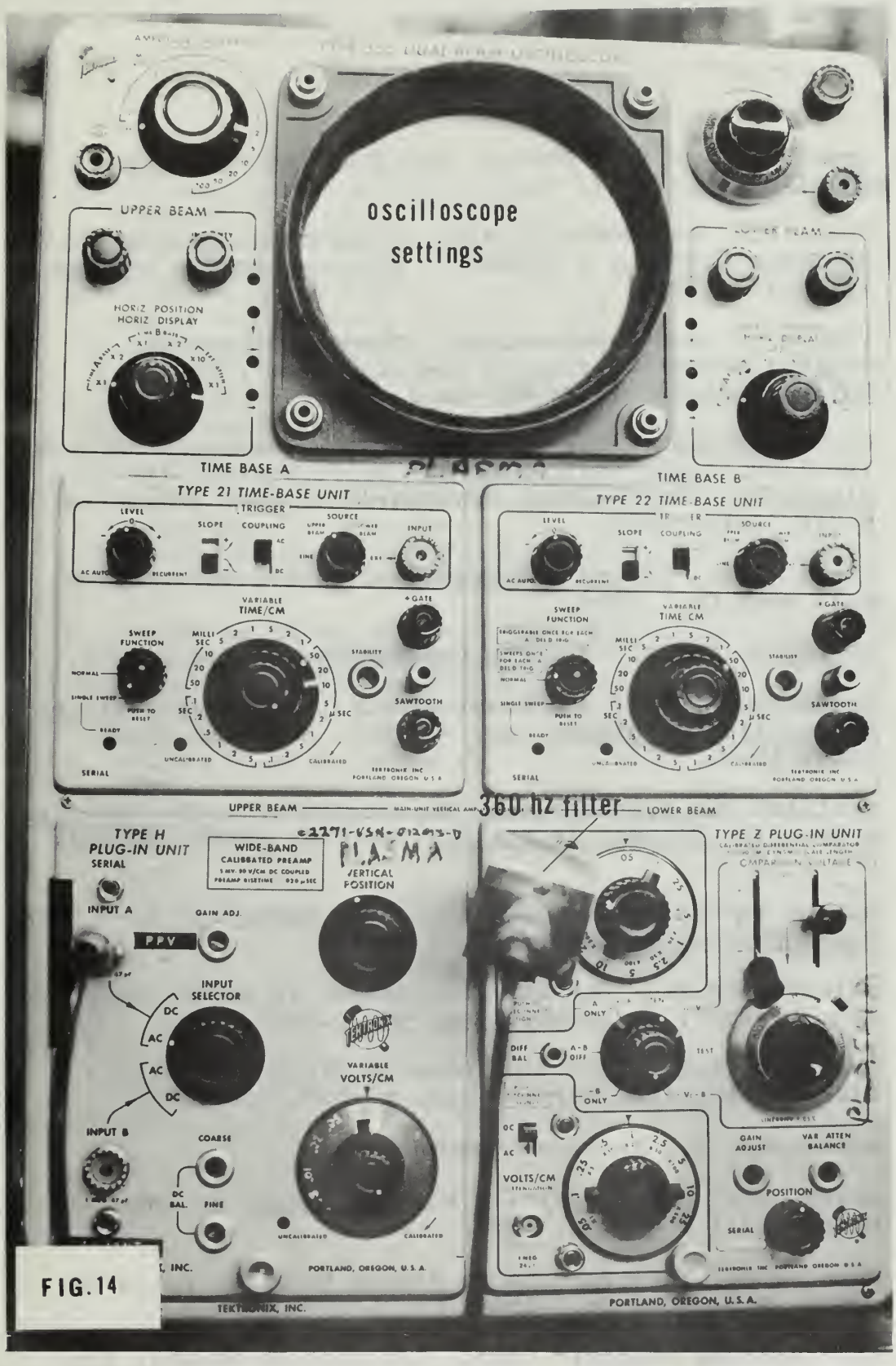
oscilloscope
settings
UPPER BEAM
HORIZ POSITION
HORIZ DISPLAY
TIME BASE A
TIME BASE B
TYPE 21 TIME-BASE UNIT
TRIGGER
LEVEL
SLOPE
COUPLING
SOURCE
INPUT
VARIABLE
TIME/CM
SWEEP
FUNCTION
+GATE
STABILITY
SAWTOOTH
SERIAL
TYPE 22 TIME-BASE UNIT
UPPER BEAM
360 hz filter
LOWER BEAM
TYPE H
PLUG-IN UNIT
SERIAL
WIDE-BAND
CALIBRATED PREAMP
PLASMA
VERTICAL
POSITION
INPUT A
GAIN ADJ.
PPV
INPUT
SELECTOR
DC
AC
INPUT B
COARSE
FINE
VARIABLE
VOLTS/CM
UNCALIBRATED
CALIBRATED
PORTLAND, OREGON, U.S.A.
TEKTRONIX, INC.
TYPE Z PLUG-IN UNIT
DIFF
BAL
A-B
DIFF
A
ONLY
B
ONLY
TEST
VOLTS/CM
GAIN
ADJUST
VAR ATTEN
BALANCE
POSITION
SERIAL
PORTLAND, OREGON, U.S.A.

FIG. 14

BIBLIOGRAPHY

1. Baird-Atomic, Inc. Manual, The Three Meter Grating Spectrograph, 1963.

2. Chan, P.W. and Nodwell, R.A., "Collective Scattering of Laser Light by a Plasma", Physical Review Letters 16, p.122, 1966.

3. Fiocco, G. and Thompson, E., "Thomson Scattering of Optical Radiation from an Electron Beam", Physical Review Letters, 10, p.89, 1963.

4. General Dynamics Corp., General Atomic Division Report 1PP 1/48, Light Scattering and Drift Instability in a Plasma by Otto Theimer, translated by Fred Schwirzke, p.2ff, July, 1966.

5. Greim, H.R., Plasma Spectroscopy, pp.180-184, McGraw-Hill Book Co., 1964.

6. HPA Corp. Manual, The PIN Photodiode, 15 Feb., 1966.

7. Huddelstone, R.H. and Stanley, L.L., (Editors), Plasma Diagnostic Techniques, pp. 594-596, Academic Press, Inc., 1965.

8. Institut Für Plasmaphysik, Report IPP/6/9, The Laser as a Tool for Plasma Diagnostics, by W.H. Kegel, pp.2ff, Oct., 1963.

9. Optics Technology, Inc. Manual, The Model 130 High Peak Power Q-switched Laser, Apr., 1966.

10. Salpeter, E.E., "Density Fluctuation in a Non-equilibrium Plasma", J. Geophys.Res. 68, p.4870, 1963.

11. Salpeter, E.E., "Electron Density Fluctuations in a Plasma", Physical Review, 120, p.1528, 1960.

13. Schwirzke, F., Personal Communication.

14. Smith, W.V. and Sorokin, P.P., The Laser, pp.151-153, McGraw-Hill Book Co., 1966.

15. Uman, M.A., Introduction to Plasma Physics, pp.33-36, McGraw-Hill Book Co., 1964.

16. Westinghouse Electric Corp., Instruction Manual, The Model RN-1 Laser Radiometer.

INITIAL DISTRIBUTION LIST

		No. Copies
1.	Defense Documentation Center Cameron Station Alexandria, Virginia 22314	20
2.	Library, Code 0212 Naval Postgraduate School Monterey, California 93940	2
3.	Naval Air Command (Code AIR-310) Department of the Navy Washington, D.C.	1
4.	Assoc. Professor Fred Schwirzke (Code 61Sw) Department of Physics Naval Postgraduate School Monterey, California 93940	1
5.	Professor N. L. Oleson (Code 610e) Department of Physics Naval Postgraduate School Monterey, California 93940	1
6.	LTJG Alfred A. Pease 4121 N. 33rd Road Arlington, Virginia 22207	1

DOCUMENT CONTROL DATA - R & D

(Security classification of title, body of abstract and indexing annotation must be entered when the overall report is classified)

1. ORIGINATING ACTIVITY *(Corporate author)*
Naval Postgraduate School
Monterey, California 93940

2a. REPORT SECURITY CLASSIFICATION
Unclassified

2b. GROUP

3. REPORT TITLE
Laser Light Scattering As a Plasma Diagnostic Technique

4. DESCRIPTIVE NOTES *(Type of report and inclusive dates)*
Master's Thesis; June 1969

5. AUTHOR(S) *(First name, middle initial, last name)*
Alfred A. PEASE

6. REPORT DATE	7a. TOTAL NO. OF PAGES	7b. NO. OF REFS
June 1969	98	16

8a. CONTRACT OR GRANT NO.	9a. ORIGINATOR'S REPORT NUMBER(S)
b. PROJECT NO.	
c.	9b. OTHER REPORT NO(S) *(Any other numbers that may be assigned this report)*
d.	

10. DISTRIBUTION STATEMENT
~~Distribution of this document is unlimited.~~ This document has been approved for public release and sale; its distribution is unlimited.

11. SUPPLEMENTARY NOTES	12. SPONSORING MILITARY ACTIVITY
	Naval Postgraduate School Monterey, California 93940

13. ABSTRACT

The effort here was concerned with initiating a long term experimental study to develop the method of laser light scattering as a plasma diagnostic technique. This was done with a ruby laser and a grating spectometer coupled with sensitive detectors, at the steady state plasma facility at the Naval Postgraduate School. Although attempts to detect the extremely low levels of scattered light failed, excellent progress was made in determining existing apparatus limitations and in recognizing which system parameter may be adjusted in order to detect the scattered light; this will enable the future experimenter to progress with a minimum of overlap.

14. KEY WORDS	LINK A		LINK B		LINK C	
	ROLE	WT	ROLE	WT	ROLE	WT
Laser Light Scattering						
Plasma Diagnostic Technique						
Scattered Spectral Distribution						